ELSEVIER

Polymer 42 (2001) 3533–3557

polymer

www.elsevier.nl/locate/polymer

Changes in molecular dynamics during the bulk polymerisation of an epoxide/boroxine mixture as studied by dielectric relaxation spectroscopy, revealing direct evidence for a floor temperature for reaction

G. Williams[a,*], I.K. Smith[a], G.A. Aldridge[a], P. Holmes[b], S. Varma[b]

[a]*Department of Chemistry, University of Wales, Singleton Park, Swansea, Wales SA2 8PP, UK*
[b]*Pilkington Technology Centre, Hall Lane, Lathom, Ormskirk, Lancashire L40 5UF, UK*

Received 24 July 2000; received in revised form 18 September 2000; accepted 26 September 2000

Abstract

Real-time dielectric relaxation spectroscopy (DRS), has been used to monitor changes in the dynamics of chain dipoles and of ions during the bulk polymerisation of an epoxide/boroxine system at different reaction temperatures T_R in the range 60–120°C. For $T_R < 72$°C the dielectric α-process moved to ultra-low frequencies indicating the formation of a chemically unstable glass. For $T_R > 72$°C the process moved from high frequencies to settle at audio or higher frequencies, giving a loss peak independent of time that indicated the formation of a chemically stable elastomer. We analysed our results in terms of changes in molecular mobility in the reaction mixture with time and have determined the *floor-temperature* T_F below which a glass is formed and above which an elastomer is formed. The DRS data were also presented as complex impedance $Z(\omega)$ which emphasises changes of ionic conductance during reaction. Below T_F the peak in the loss impedance Z''_m moved to ultra-low frequencies during reaction in a time-scale far shorter than that for the dielectric loss peak ε''_m. Comparison of the two representations of data made well above T_F show that the Z'' data become independent of time before the ε'' data. DRS data presented as dielectric permittivity $\varepsilon(\omega)$ provides a good indicator of glass-formation below T_F and of elastomer-formation above T_F. Our data are considered in relation to the TTT-diagram of Gillham and coworkers that describes the onset of gelation, glass-formation and elastomer-formation during cure and we extend this diagram to describe how T_g evolves with time for different values of T_R.

Keywords: Floor temperature; Epoxide/boroxine mixture; Dielectric relaxation spectroscopy

1. Introduction

The curing-behaviour of thermosetting polymer systems has been studied by a variety of spectroscopic techniques (IR, Raman, NMR), by dynamic-mechanical relaxation (DMTA) (e.g. Refs. [1,2]), differential scanning calorimetry (DSC) (e.g. Ref. [3]) and dielectric relaxation spectroscopy (DRS) (e.g. Refs. [4–7]). The effects of varying the cure temperature T_R on the course of reaction have been described by Gillham and coworkers [1,2] and led to their *time–temperature-transition* (TTT) *diagram* in which events such as gelation, glass-formation, full cure and phase-separation were included. According to this diagram, a limiting glass transition temperature $T_{g\infty}$ exists, which is the maximum T_g obtainable for a reaction mixture irrespective of the value chosen for T_R. Above $T_{g\infty}$ reaction proceeds to full cure, producing a material with $T_g = T_{g\infty}$. Below $T_{g\infty}$ reaction proceeds up to the point in time, known as the *vitrification point*, t_v say, at which $T_{g(system)} = T_R$ and the material becomes a glass. The reaction is effectively quenched for $t > t_v$ but may continue very slowly, with a rate depending on $T_R - T_{g\infty}$. In order to increase the extent of reaction for the glassy product, post-cure is required at temperatures above T_R. DMTA, DSC and DRS studies of thermosetting systems revealed several aspects of the TTT diagram [1–3]. Following the review by Senturia and Sheppard [5] on the use of DRS for studying the curing behaviour of thermosetting systems, most DRS studies have been concerned with systems that form a glass during isothermal cure. We recently gave a comprehensive listing of studies that use DRS for cure-monitoring [8] and noted two early studies, by Johari and coworkers [9,10] of systems that do not appear to vitrify during isothermal cure. We also gave [8] preliminary real-time DRS data for an epoxide/boroxine system which showed normal vitrification behaviour at $T_R = 60$°C and elastomer-formation at 80°C. In the

* Corresponding author.

0032-3861/01/$ - see front matter
PII: S0032-3861(00)00715-1

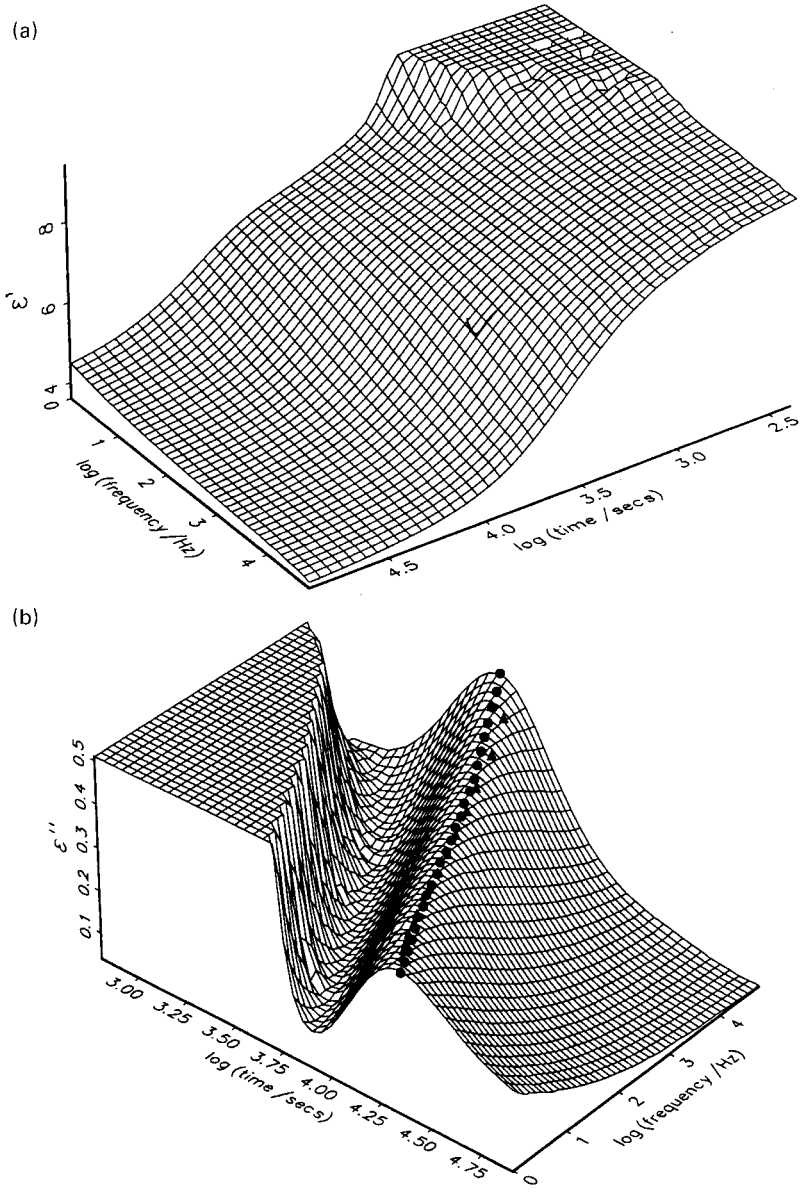

Fig. 1. Plot of (a) real permittivity ε' and (b) loss factor ε'' vs. log(*f*/Hz) and log(*t*/s) for the PY306/TMB/BA system at T_R equal to 60°C.

present paper, we report a comprehensive DRS study for the same system in which data have been obtained over a wide frequency range at eleven values of T_R in the range 60–120°C. We studied the changes that occur during reaction in: (i) the dielectric α-relaxation and (ii) the ion conductivity and show from (i) that below T_F a glass is formed and above T_F an elastomer is formed.

2. Experimental

The components chosen for the thermosetting reaction were as follows: (i) a commercially available diepoxide (Ciba-Geigy PY306); (ii) a co-reactant, cyclic trimethoxyboroxine (TMB); and (iii) an inhibitor benzyl alcohol (BA). Bulk polymerisation of a mixture of these components occurs by an ionic mechanism. Initiation occurs when the epoxide group approaches a boron atom, resulting in the creation of a new B–O bond between B on TMB and the epoxide oxygen, the release of a methoxide anion and the creation of a new active cationic centre at the secondary carbon position of the epoxide unit. Chain propagation occurs by addition of further epoxide to the cationic centre. A key termination step occurs when the methoxide anion removes a H-atom from the carbon atom adjacent to the cationic centre, resulting in the formation of an alkene bond and a methanol molecule. The presence of three boron atoms in the TMB-ring and the bifunctionality of PY306 results in the formation of a highly cross-linked polymer. For our

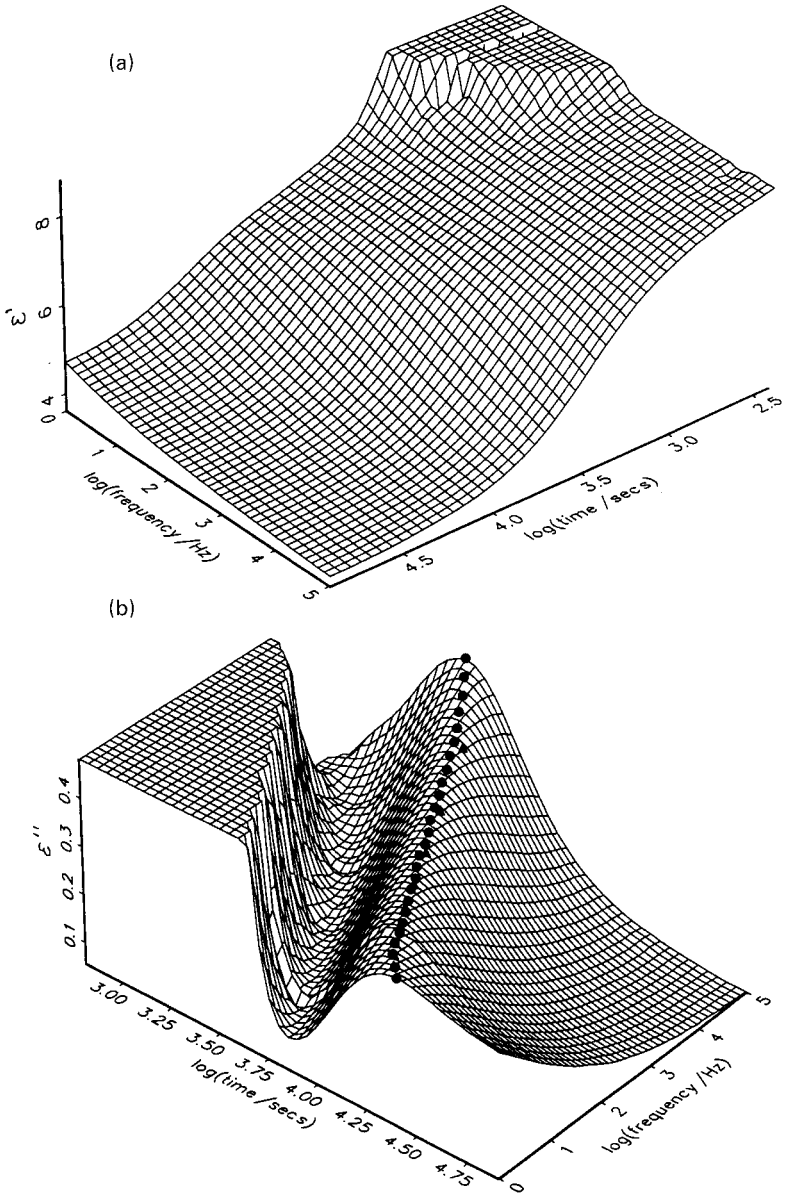

Fig. 2. Plot of (a) real permittivity ε' and (b) loss factor ε'' vs. log(f/Hz) and log(t/s) for the PY306/TMB/BA system at T_R equal to 65°C.

studies each sample of the PY306, TMB and BA mixture was made up in the ratio 14:3:1 by weight (w/w) and was stirred for 5 min at 50°C to ensure homogeneity. Initially, a mixture was a white liquid of medium viscosity but became clear and had a lower viscosity after stirring. The sample was poured into the parallel-plate electrode assembly [8] then placed into a Novocontrol BDS 1200 sample holder that had been pre-heated to T_R. DRS measurements were performed at a chosen reaction temperature T_R using a Novocontrol dielectric spectrometer that incorporated a Solartron 1260 Frequency–Response-Analyser operated under computer control. Opening and positioning the sample in the Novocontrol cryostat/heating chamber lowered the chamber-temperature from its preheated value. DRS measurements were initiated from the time at which the temperature of the chamber re-registered the chosen value of T_R. For samples cured isothermally in the range 60–95°C the DRS measurements were made at 26 frequencies in the range $1–10^5$ Hz. The real permittivity and loss factor ε'' were measured at each frequency and the time (t_r) of each measurement was recorded. Each frequency sweep took $\approx$ 3.5 min. In order to monitor the reaction fairly continuously, frequency-sweeps were initiated every 4 min. For samples cured in the range 100–120°C, variable f-ranges combined with variable sweep-times (120–390 s) allowed the conductivity variations at short times to be monitored accurately. Three-dimensional (3D) plots of permittivity or loss vs. log f and t_r were constructed using an Axum programme.

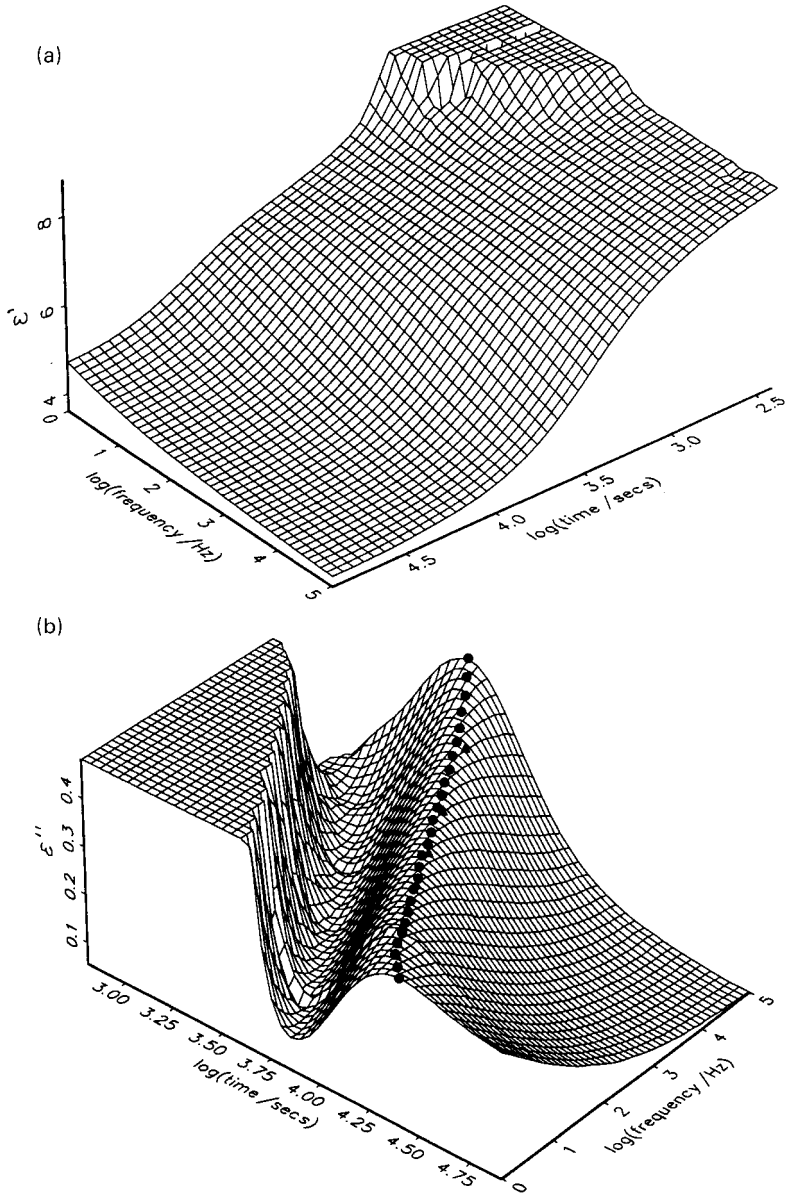

Fig. 3. Plot of (a) real permittivity ε' and (b) loss factor ε'' vs. log(*f*/Hz) and log(*t*/s) for the PY306/TMB/BA system at T_R equal to 70°C.

3. Results and discussion

Figs. 1–11 show 3D plots of ε' and ε'' vs. log(*f*/Hz) and $\log_{10}(t_r/s)$ for isothermal cures conducted at the eleven temperatures in the range 60–120°C (Figs. 1 and 5 were shown in our preliminary publication, Ref. [8], and are reproduced here with permission). Ionic conductivity and electrode polarisation due to ionic species gives the increase in ε' and ε'' at low frequencies. The importance of these effects due to ions decreases rapidly with increasing t_r since ion mobility decreases as the local viscosity of the mixture increases during reaction. At longer times, the ε' values decrease from those typical of a liquid and ε'' shows a well-defined peak (see e.g. Fig. 1) due to the α-relaxation process, which arises from the large-scale motions of dipoles associated with polymeric and monomeric species in the mixture. The movement of the α-process towards ultra-low frequencies with time (e.g. for $T_R = 60$°C (Fig. 1b)) indicates *premonitory behaviour* of the formation of a glass at longer times. At higher temperatures qualitatively different behaviour is observed, as was made clear in our preliminary publication [8]: e.g. at $T_R = 80$°C the peak for the α-process moved initially from high frequencies as if it were headed for ultra-low frequencies but then it settled to give loss-curves that are independent of time with a constant average relaxation time $\langle\tau_\alpha\rangle = [2\pi f_{max}]^{-1}$ where f_{max} is the frequency of maximum loss for a given time t_r. Such behaviour is rationalised as follows. At 60°C, molecular mobility decreases during reaction until it becomes so slow that the chemical reaction rate becomes diffusion-controlled. The

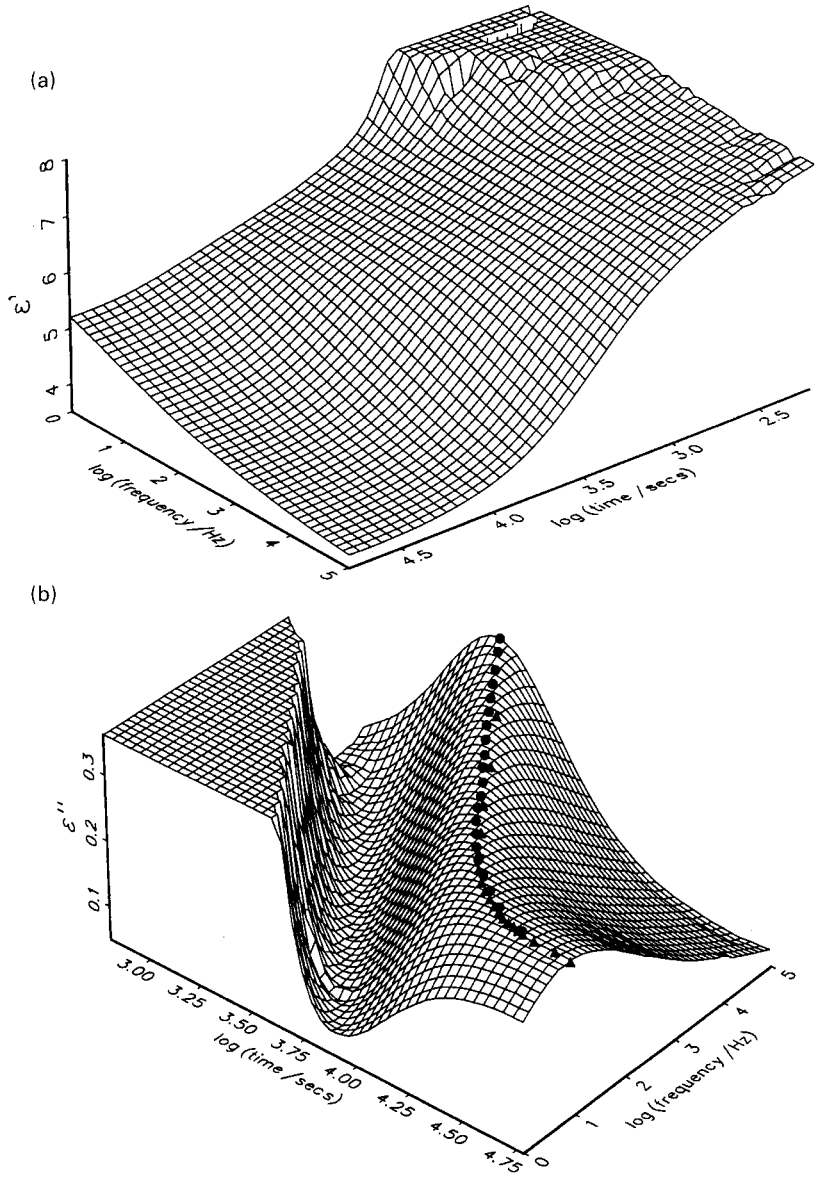

Fig. 4. Plot of (a) real permittivity ε' and (b) loss factor ε'' vs. log(f/Hz) and log(t/s) for the PY306/TMB/BA system at T_R equal to 75°C.

chemical kinetics are modified in the diffusion-controlled regime, as we have discussed [8], so a glass is formed at long times. The product is formed before completion of the chemical reaction and further reaction will occur if the glassy sample is post-cured [3]. The chemical kinetics of a thermosetting reaction in which a glass is formed was modelled by us [11] to include a diffusion-control term based on a Fermi–Dirac function. At 80°C (Fig. 5b), the loss peak moves initially from high to low frequencies as at 60°C, but then stabilises, becoming independent of time after ~40 ks. The fact that the loss spectra are independent of time at the longest times at $T_R = 80$°C means that reaction is able to reach completion at this temperature since molecular mobility is sufficient at all times. This is evident from the work of Montserrat [3] who showed for a thermosetting reaction that both the limiting long-time conversion α_∞ and T_g(product) increased with increasing T_R for $T_R < T_{g\infty}$, due to the effects of diffusion-control on reaction rate, but were independent of T_R for $T_R > T_{g\infty}$ since reaction could be completed if the product was an elastomer, i.e. if the effect of glass-formation on reaction rate was avoided (see Figs. 3 and 4 of Ref. [3]). So the effects of diffusion-control associated with reduced molecular mobility, which were evident at 60°C are not involved at 80°C. The dielectric spectra at 80°C in Fig. 5b (see also Fig. 9, Ref. [8]) show that a the system transforms from a mobile liquid to a mobile *elastomer* (the limiting value of log(f_m/Hz) at long times for the α-process is ~8 Hz). The DRS behaviour shown in Figs. 3–11 for T_R in the range 70–100°C is qualitatively different from that reported [8] in most DRS studies of curing systems where glassy products were obtained.

As explained, the DRS measurements recorded paired

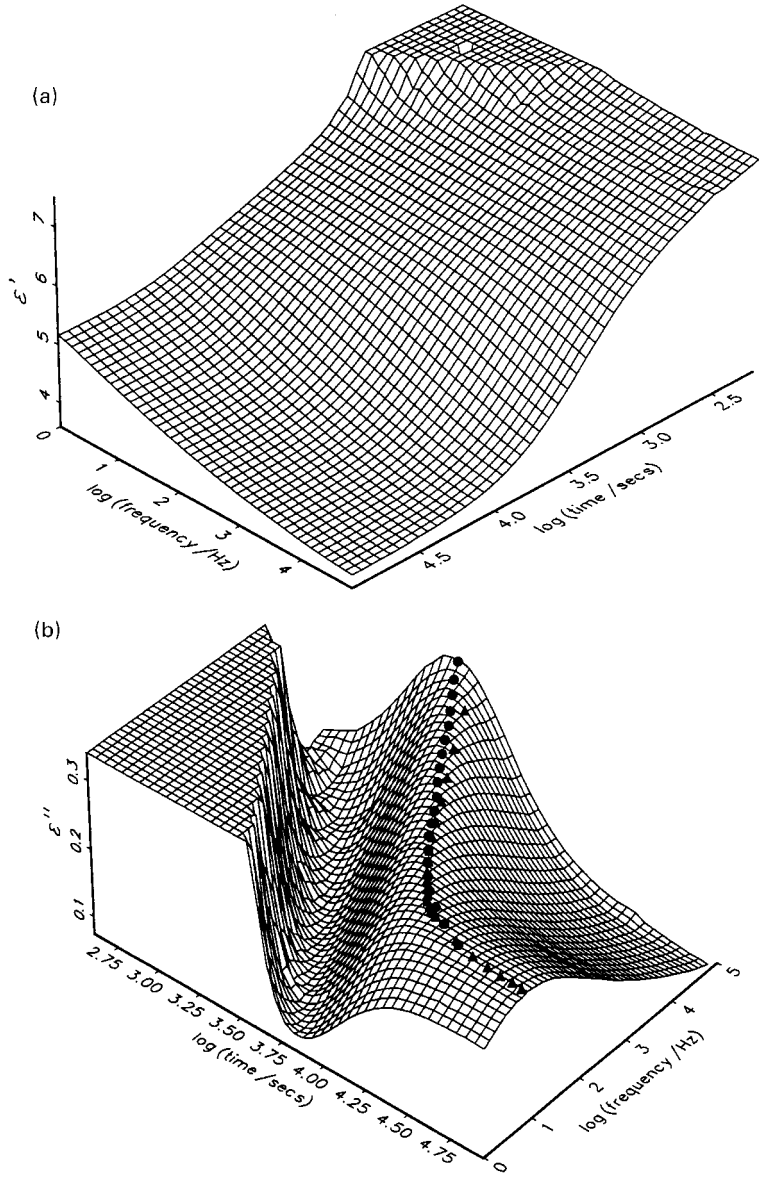

Fig. 5. Plot of (a) real permittivity ε' and (b) loss factor ε'' vs. log(f/Hz) and log(t/s) for the PY306/TMB/BA system at T_R equal to 80°C.

values [ε',ε''] at a measuring frequency f and a reaction time t_r. These data immediately yield plots of ε' and ε'' vs. t_r for given frequencies (plots A, say). Plots of ε' and ε'' vs. log f at fixed times t_r (plots B, say) were derived by manual interpolation of these data and represent the DRS behaviour of a chemically and physically 'arrested state' of the reaction mixture at each time t_r. We have determined the times of maximum loss, t_m, for given frequencies from plots A and the frequencies of maximum loss, f_{max}, for given times t_r from plots B. These points are shown overlaid in Figs. 1b–9b as ● for t_m and ▲ for f_{max}. The loci for ● and ▲ are similar where both are observable. When the loss curves become independent of time at long times, t_m ceases to have meaning since ε'' at a fixed frequency rises to a plateau value with time. See Fig. 5b which shows that at 80°C a peak is obtained in the plot of ε'' vs. t_r for 10^2 Hz $< f <$ 10^5 Hz but is not observed for $f \leq 10$ Hz. This will be discussed further below. The loss curves at 110 and 120°C (Figs. 10 and 11) show only the low frequency side of the α-relaxation in our range. In summary, the dielectric α-process moves rapidly to very low frequencies with time at 60 and 65°C indicating glass-formation while at the higher temperatures it settles to become independent of time with the peak position at medium to high frequencies, showing that an elastomer is formed.

In previous papers [8,11], we described the evolution with time of the DRS behaviour for dipole motions in thermosetting systems. According to Cassettari et al. [12,13] and Casalini et al. [14] the dielectric αβ-process for the unreacted monomer mixture transforms into α and β processes as reaction proceeds. The higher frequency (β) process is due to local motions of dipolar species and relaxes

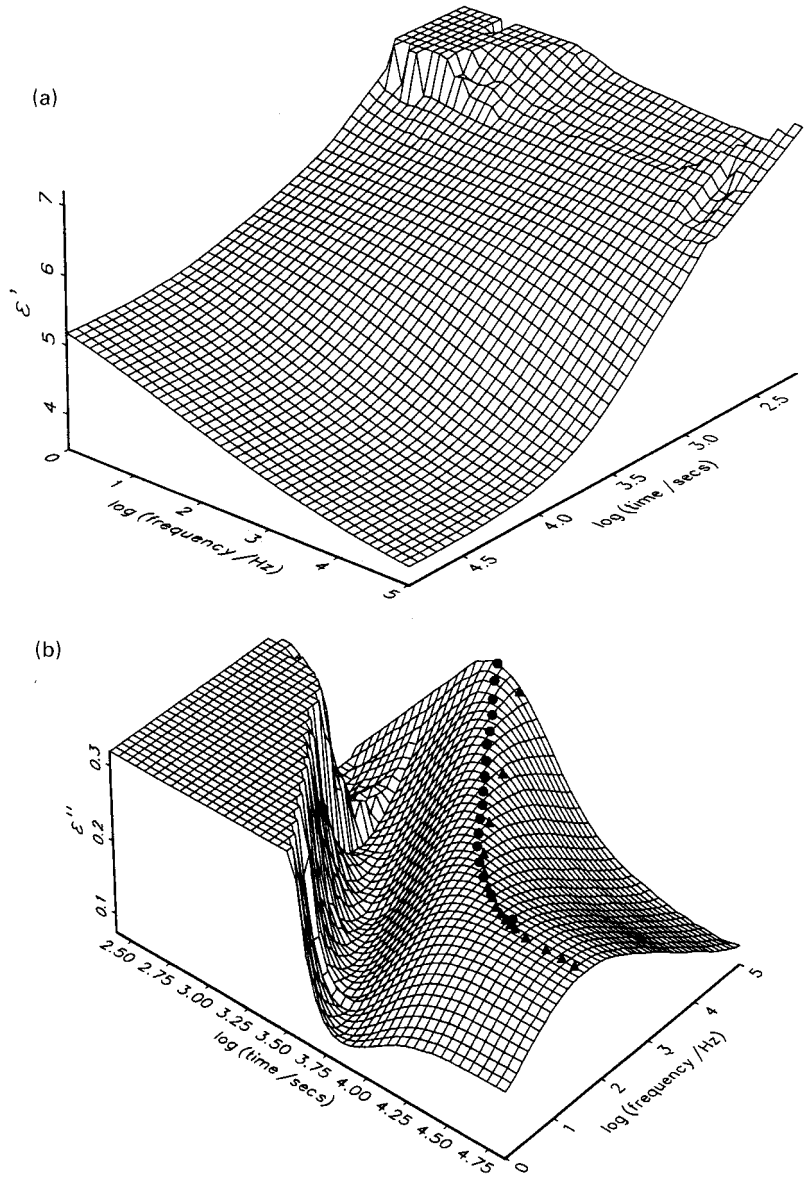

Fig. 6. Plot of (a) real permittivity ε' and (b) loss factor ε'' vs. log(f/Hz) and log(t/s) for the PY306/TMB/BA system at T_R equal to 90°C.

only a part, $\Delta\varepsilon_\beta$, of the total relaxation strength $\Delta\varepsilon$. The lower frequency (α) process is due to the large-scale cooperative motions of all dipolar species and relaxes the remainder $\Delta\varepsilon_\alpha = \Delta\varepsilon - \Delta\varepsilon_\beta$.

If α and β relaxations are fully observable in plots of ε'' vs. log f for a given t_r then linear response theory, that relates the complex dielectric permittivity $\varepsilon(\omega,t_r)$ to the time correlation function $[\Phi_\mu(t)]_{t_r}$, may be applied as follows [8]

$$\frac{\varepsilon(\omega,t_r)-\varepsilon_\infty(t_r)}{\varepsilon_0(t_r)-\varepsilon_\infty(t_r)} = 1 - i\omega\Im[\Phi_\mu(t)]_{t_r} \quad (1)$$

$\Im$ indicates a one-sided Fourier transform, $\varepsilon_0(t_r)$ and $\varepsilon_\infty(t_r)$ are, respectively, the limiting low and high frequency real permittivities with respect to the entire relaxation region and $[\Phi_\mu(t)]_{t_r}$ is the dipole moment time-correlation function at t_r for all dipoles in a macroscopic volume V of the mixture and includes the equilibrium and dynamic auto and cross-correlation terms for all the dipoles [15,16]. In Appendix A, we give the following relation for $\varepsilon(\omega,t_r)$ for a reacting system in which the α and β relaxations are observable in the f-domain at a reaction time t_r.

$$\frac{\varepsilon(\omega,t_r)-\varepsilon_\infty(t_r)}{\varepsilon_0(t_r)-\varepsilon_\infty(t_r)} = A_\alpha(t_r)S_\alpha(\omega,t_r) + A_\beta(t_r)S_\beta(\omega,t_r) \quad (A4)$$

A_i and S_i are the normalised relaxation strength and relaxation function, respectively, for process i ($i = \alpha$ or β) and are defined in Appendix A. The β process is a weighted sum of local partial re-orientational processes for the dipoles and relaxes only a part of the total relaxation strength. The α process relaxes the remainder of $\Delta\varepsilon(t_r)$ as a weighted sum of

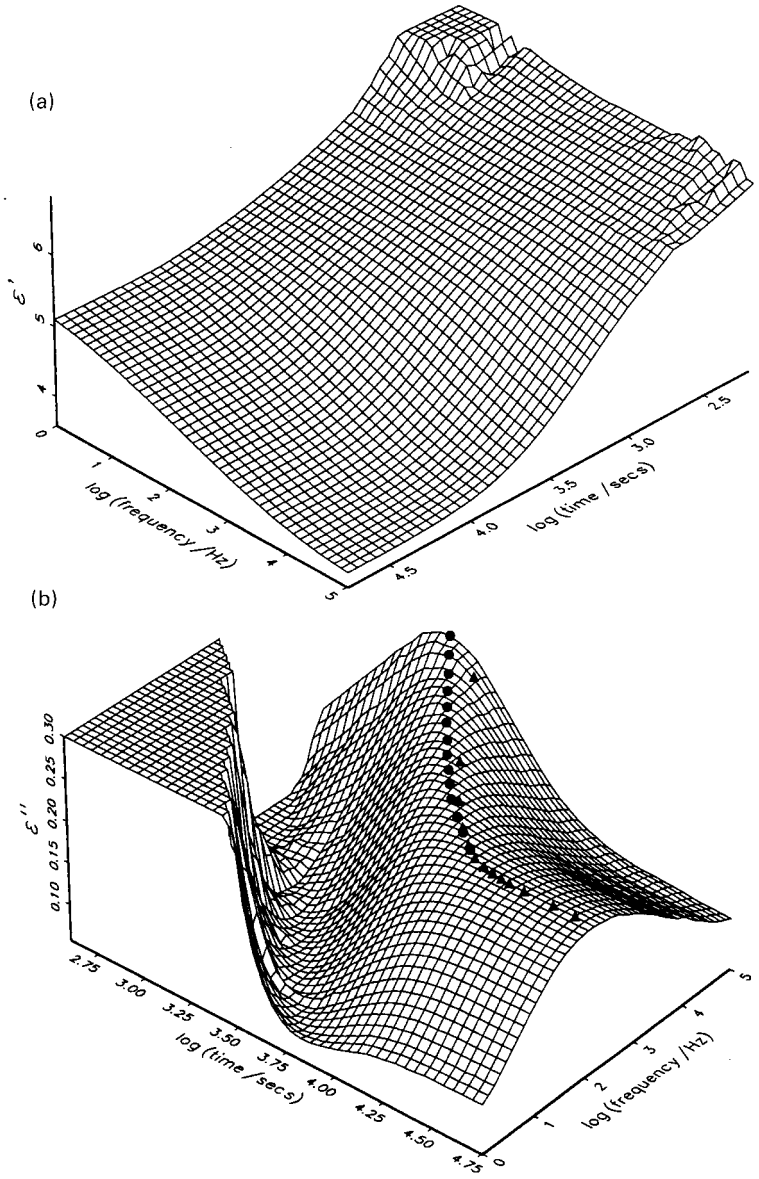

Fig. 7. Plot of (a) real permittivity ε' and (b) loss factor ε'' vs. log(f/Hz) and log(t/s) for the PY306/TMB/BA system at T_R equal to 95°C.

α-processes for the different dipoles. For the present system, we observed the behaviour of the α-process which has a relaxation strength

$$\Delta\varepsilon_\alpha(t_r) = [(\varepsilon_0(t_r) - \varepsilon_\infty(t_r)]A_\alpha(t_r) \quad (2)$$

where $A_\alpha(t_r)$ and $S_\alpha(\omega,t_r)$ are given by Eqs. (A5a) and (A5c), respectively. Thus, the α-process relaxes the *mean dipole moment* residing in each group after the local motions (β-process) have occured. Figs. 1–11 give information on the changes that occur in $\Delta\varepsilon_\alpha(t_r)$ and $S_\alpha(\omega,t_r)$ during reaction. $S_\alpha(\omega,t_r)$ gives information on changes in the mean relaxation time $\langle\tau_\alpha(t_r)\rangle = [1/2\pi f_{max}(t_r)]^{-1}$ and the effective distribution of relaxation times for this process. As we have indicated, the α-process exhibits two types of behaviour during reaction, depending on T_R: (A) where the peak moves to ultra-low frequencies with time; and (B) where the peak stabilises at long times. We now consider the changes of the α-process in greater detail.

4. Evolution of the α-process

As examples, Figs. 12–15, show DRS data at 60 and 80°C.[1] Figs. 13 and 15 were derived from the iso-frequency data of Figs. 12 and 14 and show how the relaxation strength and relaxation function changes with time. ε_0-values in Figs. 13a and 15a are ~7.2 and 5.9, respectively, while $\varepsilon_{\infty\alpha}$ is ~3.7 at these temperatures. Typical values of ε_∞ for organic media lie in the range 2.2–2.5, so $\Delta\varepsilon_\alpha > \Delta\varepsilon_\beta$ for the present system. In Figs. 12a and 14a, $\varepsilon_0(t_r)$ forms the

[1] Shown in Ref. [8], reproduced with permission.

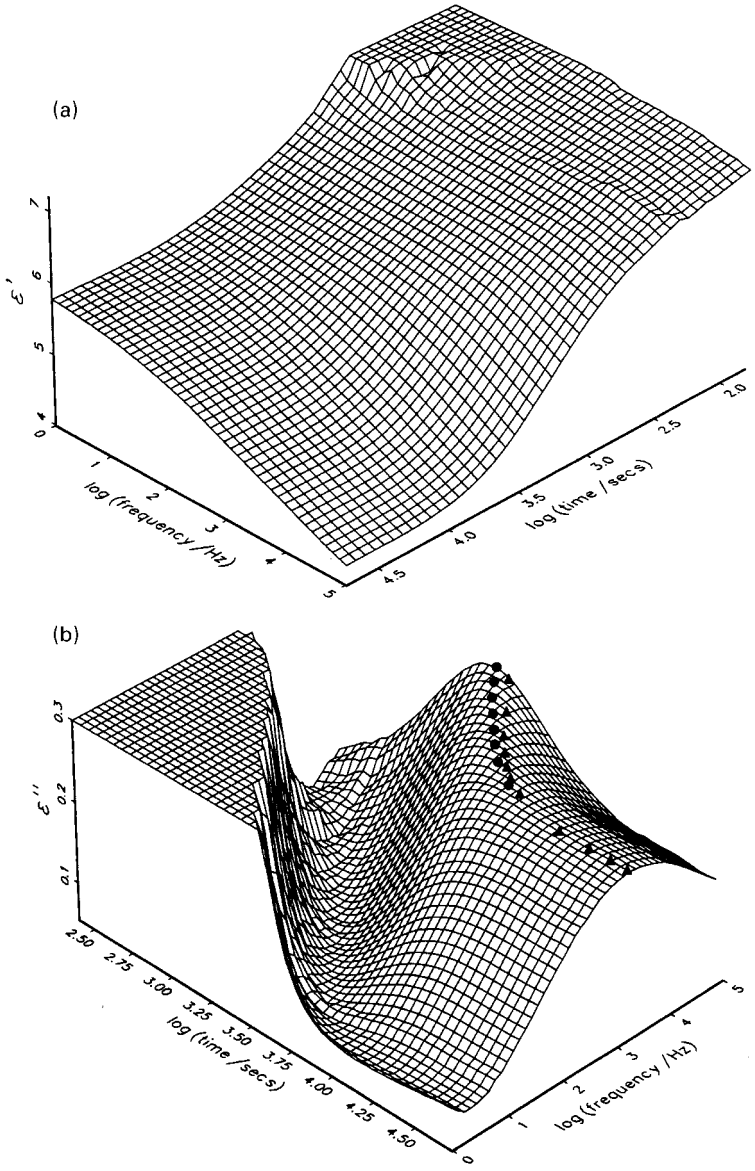

Fig. 8. Plot of (a) real permittivity ε' and (b) loss factor ε'' vs. log(f/Hz) and log(t/s) for the PY306/TMB/BA system at T_R equal to 100°C.

common line, independent of frequency, observed at times: (i) greater than those in which ε'-values increase markedly with decreasing frequency due to conduction effects; and (ii) less than those in which ε' values decrease due to the α-process. So $\varepsilon_0(t_r)$, and thus $\Delta\varepsilon$ and $\Delta\varepsilon_\alpha$, decrease with increasing t_r at these temperatures, in accord with previous DRS studies of epoxide–amine thermosetting systems [8,12–14]. At 60°C the ε_0 values fall from 9.0 to 7.0 as log(t_r/s) increases from 2.5 to 4.0, while at 80°C ε_0 falls from 7.0 to 5.95 in the same range. Since $\Delta\varepsilon$ decreases with time the epoxide and amine dipole groups are being replaced by groups having lesser dipole strength and/or lesser spatial extent of motion (e.g. as at cross-links). Johari and coworkers [17,18] (see also Refs. [16–26] in Ref. [8]) plot the Argand diagram ε'' vs. ε' for a fixed measuring frequency during reaction of different thermosetting systems and have used a form of the KWW relaxation function [19] to fit their data. Butta et al. [21] have commented that such plots are not equivalent to plots of ε'' vs. ε' at fixed t_r values and different frequencies. Johari and coworkers have defended their approach [22], but difficulties remain, as we have discussed [8]. The procedure of Johari and coworkers is analogous to the time–temperature superposition principle used for relaxation in stationary systems [20,23]. The superposition of a set of relaxation curves of [ε',ε''] vs. log ω for a stationary system at different temperatures to form a master curve requires: (i) horizontal shifting of each curve by the factor log[$a(T)$] to account for changes in relaxation time; and (ii) vertical shifting to accommodate changes in ε_0 and ε_∞. Master curves for stationary systems as plots of [ε',ε''] vs. log[$a(T)$] can be obtained, giving a master plot for ε'' vs. ε'. For a reacting

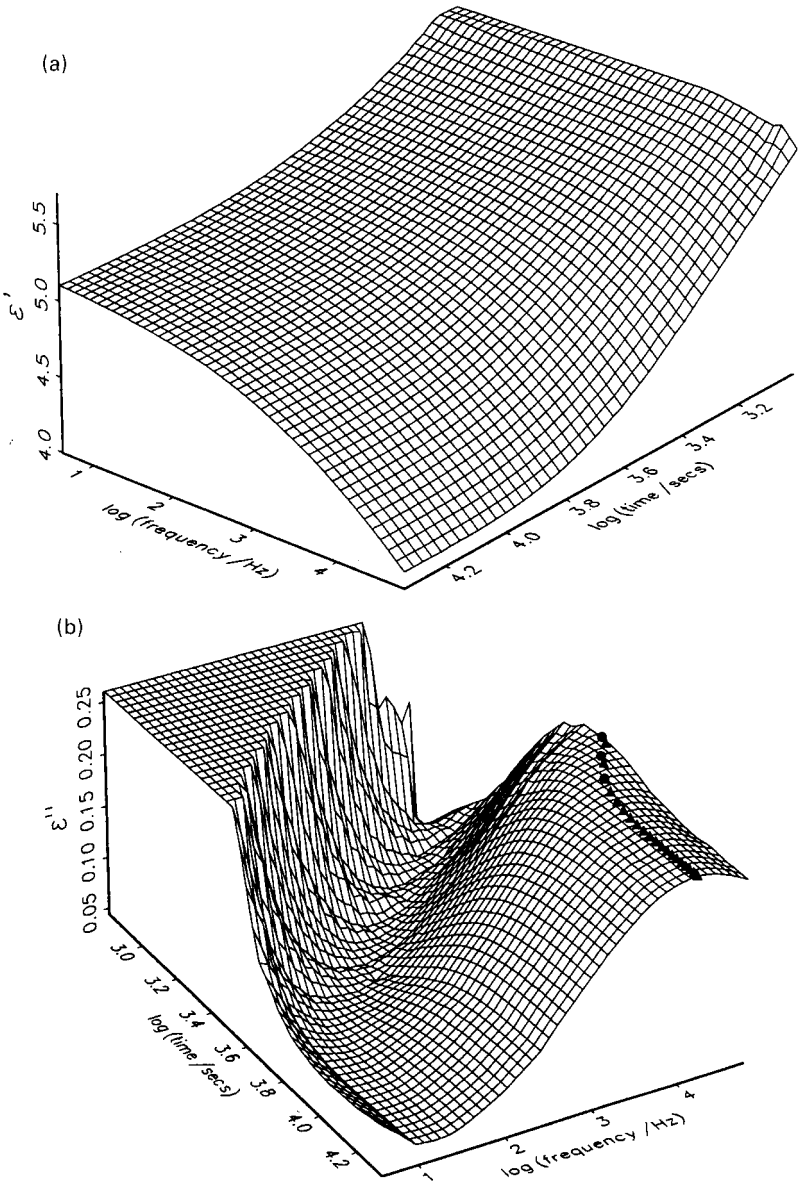

Fig. 9. Plot of (a) real permittivity ε' and (b) loss factor ε'' vs. log(f/Hz) and log(t/s) for the PY306/TMB/BA system at T_R equal to 110°C.

system the plot of the dielectric properties vs. time at a fixed frequency during reaction will only produce a master curve for the Argand diagram if: (i) $\varepsilon_0(t_r)$ and $\varepsilon_{\infty\alpha}(t_r)$ are independent of t_r; and (ii) the shape of the relaxation function $S_\alpha(\omega,t_r)$ is independent of t_r in the relaxation region. Our data show that $\varepsilon_0(t_r)$ decreases by ~25% in the range $2.5 < \log(t/s) < 4.0$. Taking $\varepsilon_{\infty\alpha}(t_r)$ to be approximately constant at ~3.8 from Figs. 12 and 13 we estimate that $\Delta\varepsilon_\alpha(t_r)$ changes by 50% in this range. Thus substantial vertical corrections may be necessary to scale $\varepsilon_0(t_r)$ to form a master Argand plot for the present system. However the use of scaled Argand plots for DRS data with variable t_r at fixed frequencies are unnecessary since the DRS data were obtained over a wide frequency range at fixed reaction times. Fig. 13a and b show plots of ε' and ε'' vs. log(f/Hz) at $T_R = 60$°C. The loss peaks move steadily to low frequencies, decreasing in height on going from 4 to 10 ks, reflecting a change in both $\Delta\varepsilon_o(t_r)$ and $S_\alpha(\omega,t_r)$ with t_r in this range. We estimate, that $\varepsilon_o(t_r)$ decreases from 6.85 to 6.60 in the range 10–20 ks (Fig. 12a) while ε''_{max} decreases from 0.365 to 0.350 (Fig. 13b). The shape of the loss curves is nearly unchanged with t_r in this range so if a small vertical correction is applied to the $[\varepsilon',\varepsilon'']$ data the dispersion and absorption curves obey the equivalent of the time–temperature or frequency-temperature superposition processes in this limited range of t_r. Similar conclusions apply to the data at 80°C. For $T_R = 60$°C and $t_r > 20$ ks the loss curves move to ultra-low frequencies showing that a glass is formed, but for $T_R = 80$°C the loss peaks settle at long times to become constant. Since $f_{max} \approx 8$ Hz the product is an elastomer.

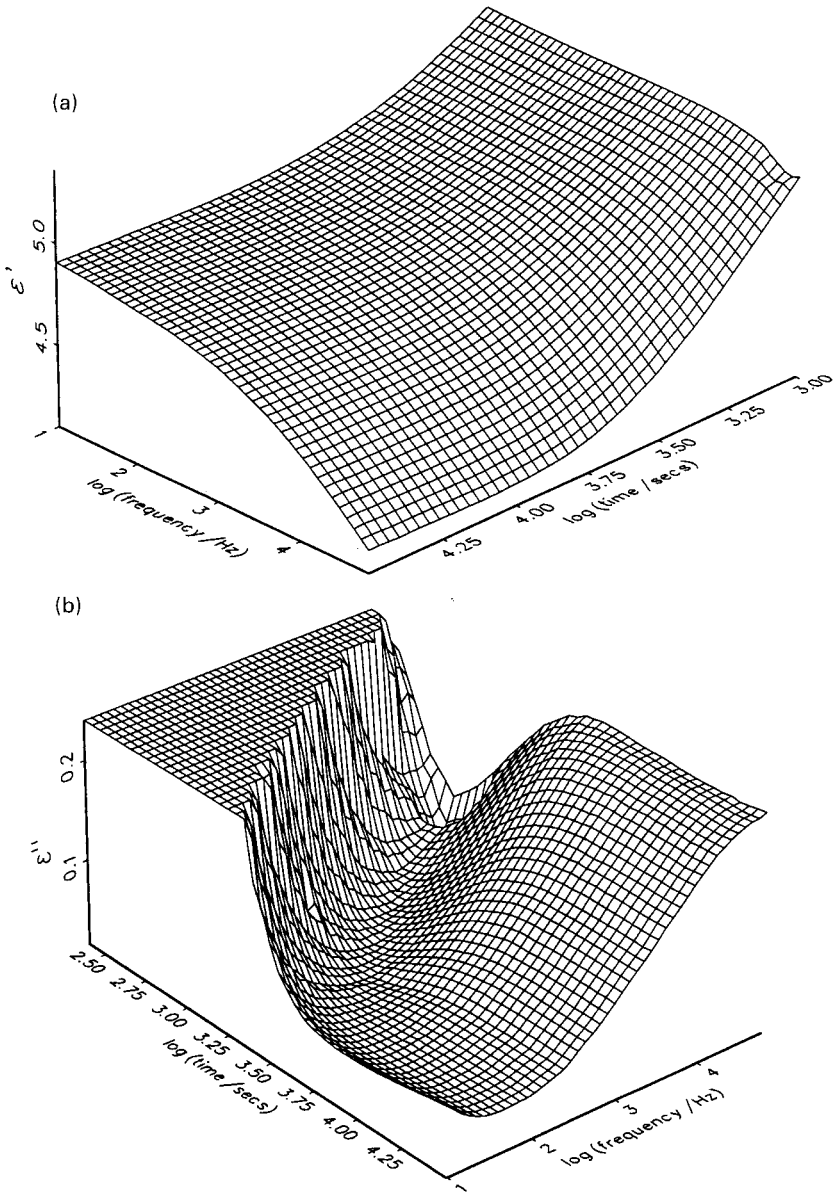

Fig. 10. Plot of (a) real permittivity ε' and (b) loss factor ε'' vs. log(f/Hz) and log(t/s) for the PY306/TMB/BA system at T_R equal to 120°C.

5. Effect of t_r on the frequency location of the α-relaxation

The times of maximum loss (t_{max}) for fixed measuring frequencies, as derived from Figs. 12b and 14b and their equivalents at different values of T_R, are shown in Fig. 16. As for other thermosetting systems that form a glass [8], the peaks at 60°C move steadily to long times with decreasing frequency. The results at 80°C and higher temperatures are qualitatively different. Fig. 14b shows that at 10^5 and 10^4 Hz the behaviour is similar to that in Fig. 12b, but as frequency is reduced to 10^3 and 10^2 Hz while a loss peak is obtained the loss values become constant at long times. At 10 and 1 Hz no loss peak is observed, the loss values rise to plateau levels with increasing t_r. Such behaviour was unexpected but was clarified when the isochronal plots were constructed (Fig. 15) that showed the α-process moves initially to low frequencies but then stabilises beyond 40 ks to become invariant with time and an elastomer is formed. Reactions conducted above 80°C give the same behaviour. These results indicate two types of behaviour for this mixture [8]. Below a *floor temperature* T_F, diffusion control of reaction, due to diminished molecular mobility, leads to the formation of a chemically unstable glass. Above T_F the material is a liquid or elastomer at all times so reaction goes to completion. Note that at high frequencies the changes of t_{max} with frequency are similar for 60 and 80°C (Figs. 12b and 14b). Extrapolation of the location of the loss peaks at short times to longer times in Fig. 14b would predict, incorrectly, that a glass is formed at long times. Thus measurements of $\varepsilon(\omega,t_r)$ for thermopolymerising

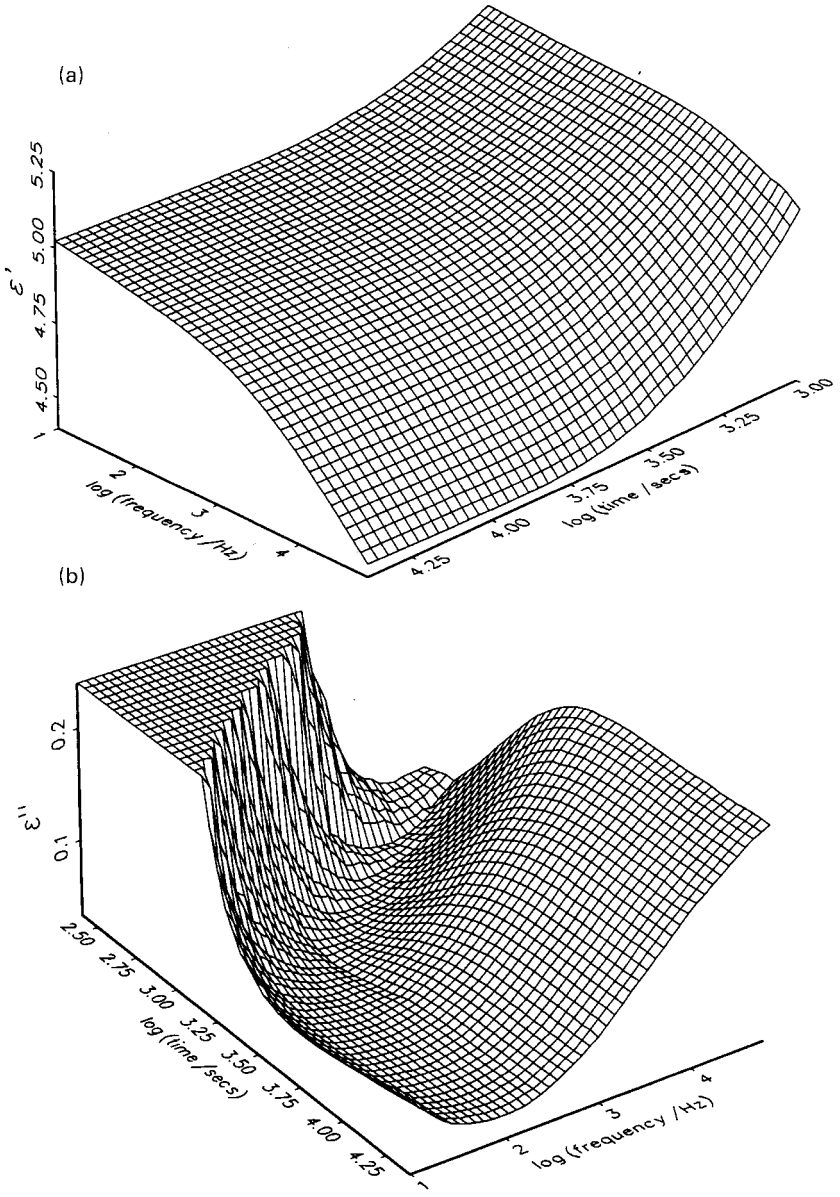

Fig. 11.

systems need to be made down to the f-range where glass-formation is apparent (i.e. $f < 1$ Hz).

In Fig. 16, for $T_R > T_F$ the plots are truncated at long times since loss peaks are not observed at the lower frequencies (e.g. for $f < 10^2$ Hz at $T_R = 80$°C, see Fig. 14b). For the short-time region in Fig. 16b the plots are linear and we write

$$f = C \exp[-g \cdot \ln t_{max}] \quad (3)$$

where the parameters C and g depend on T_R. This contrasts with the behaviour of epoxide/amine systems for which plots of $\log f$ vs. t_{max} are approximately linear [8].

Consider now the *isochronal* data e.g. as in Figs. 13 and 15. The derived plots of $\log f_{max}$ vs. t_r and $\log f_{max}$ vs. $\log t_r$ are shown in Fig. 17. The decrease in $\log f_{max}$ with increasing $\log t_r$ is approximately linear over most of the range at 60, 65 and 70°C, but there is upward curvature at the lowest frequencies. Above these temperatures the plots are linear initially then reach a plateau when the system becomes stationary. Fig. 17 includes only those points for which ε''_{max} was observed in plots of ε'' vs. $\log f$ at constant t_r. Assuming that the loss curves for $t_r > 20$ ks (Fig. 13b) move to low frequencies without an appreciable change in height and shape, $\log f_{max}$ values were determined at long times from the horizontal shift-factors relative to the data at shorter times. Table 1 gives the values determined in this way for $T_R = 60$°C. The plot of $\log f_{max}$ vs. $\log t_r$ (not shown) is linear in the range $3.75 \geq \log f_{max} \geq 0.25$ then deviates upwards at lower frequencies. The deviations $\Delta =$ [$\log f_{max}$(observed) − $\log f_{max}$ (linear plot)] are listed in

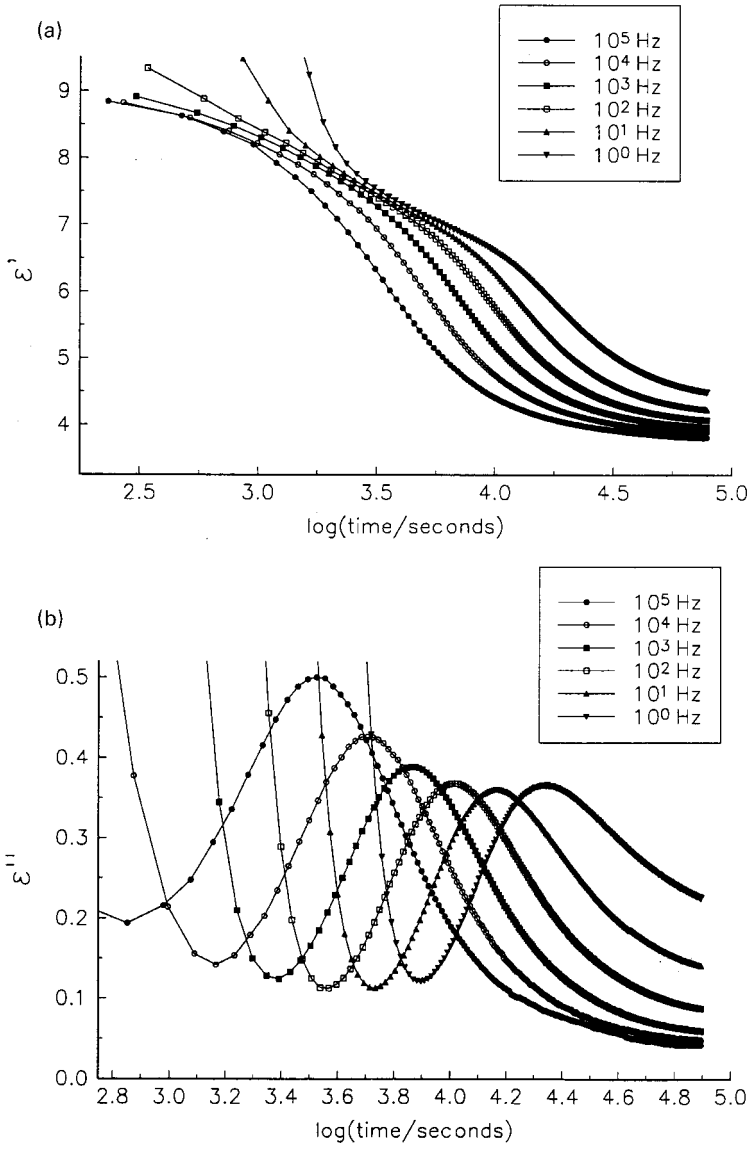

Fig. 12. (a) ε' and (b) ε'' vs. log(t/s) at fixed measuring frequencies for $T_R = 60°C$.

Table 1 and indicate *premonitory behaviour* for the occurrence of a plateau in $\log f_{max}$ below our range at very long times. At 60°C, when molecular motions become very slow ($t_r > 20$ ks, see Fig. 17) diffusion-control resulting from limited molecular mobility leads to a marked reduction in the reaction rate [8,11]. The mixture is in a non-equilibrium state with respect to its volume, enthalpy and entropy thus, as for a glass-forming liquid or amorphous polymer cooled from the melt into the glass-transition region, volume relaxation by physical ageing [24,25] will occur after the glass has been formed, even though the reaction has been arrested. The relaxation behaviour of a glass in which the structure is temporarily 'frozen-in' has been discussed by Ediger, Angell and Nagel [26] who show dielectric data for $\langle\tau_\alpha(T)\rangle$ for polyvinylmethyl ether that deviate away from the equilibrium line for $T < T_g$. They note that enthalpy relaxation data show similar behaviour. For the present case, it seems likely for $t_r > 50$ ks (Fig. 13b) that a decrease of $\log f_{max}$ towards the values extrapolated for the *linear plot* (see Table 1) would occur as volume relaxation takes place. It would be of interest to make simultaneous DRS and volume measurements in the vitrification range in order to see how $\log f_{max}$ changes during the physical ageing process for a newly-formed glassy-product of reaction. A decrease in volume should give a decrease in $\log f_{max}$ — as expected from the effect of pressure on the dielectric α-relaxation in amorphous polymers [27,28].

We define a *floor temperature* T_F as the temperature above which the reaction proceeds to form an elastomeric product. Below T_F limited mobility of reactants leads to the formation of a glass. Before we analyse the present DRS data, it is of interest to consider the work of Montserrat [3] who used DSC to study the reaction of the diglycidyl ether of bisphenol A (DGEBA) with a hardener derived from

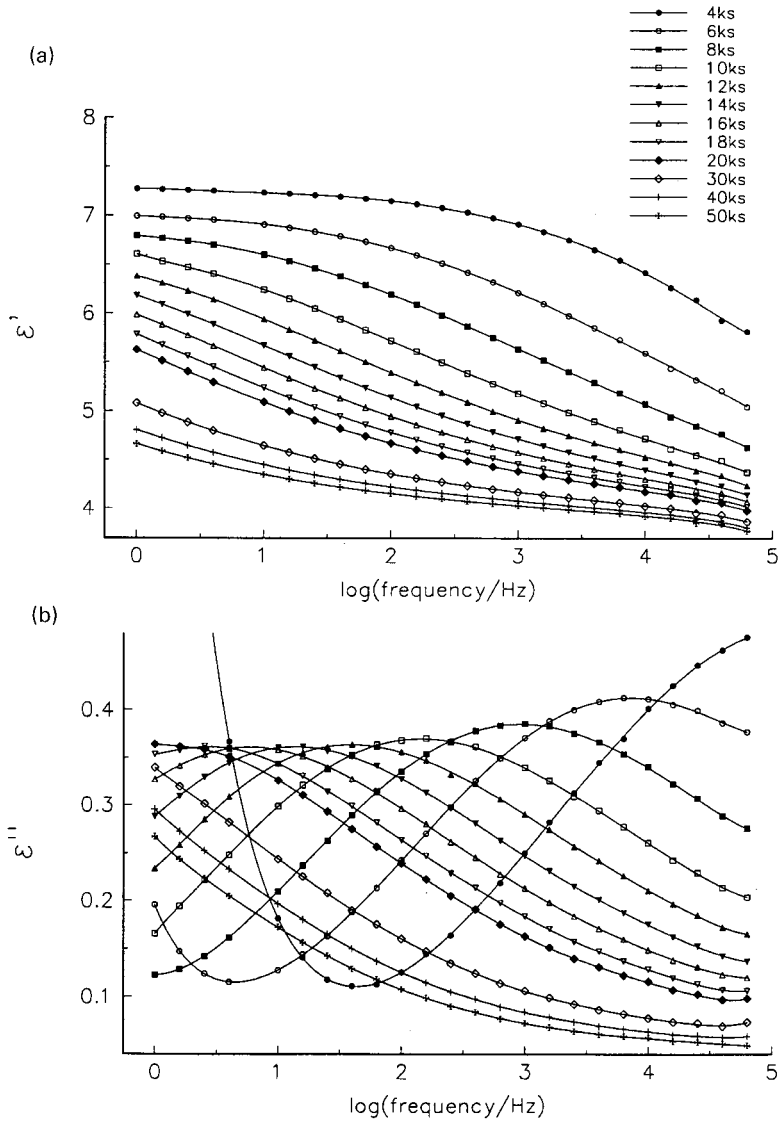

Fig. 13. (a) ε' and (b) ε'' vs. log(f/Hz) at fixed times for $T_R = 60$°C.

phthalic anhydride. Figs. 2 and 4 in Ref. [3] show plots of: (a) the conversion $\alpha(t)$ and (b) the T_g(product) vs. t_r for reactions conducted in the range 30–130°C. The limiting conversions at long times, $\alpha_L(T_R)$ say, may be determined from (a). The derived plot of α_L vs. T_R shows that $\alpha_L = 0$ for $T_R > 91 \pm 1$°C. The T_g(product) values at long times ($t = 3 \times 10^2$ h) are determined from (b) and the derived plot of T_g(product) vs. T_R shows that it reaches its limiting value $T_{g\infty}$(= 109°C) at 91 ± 1°C. We conclude that there is a floor temperature $T_F = 91 \pm 1$°C for this reaction mixture, above which an elastomer is formed and conversion goes to completion. The relationship of $T_{g\infty}$(= 109°C) to T_F(= 91°C) is unclear since T_g(DSC) is a dynamic quantity obtained from scans at a heating rate of 10 K min^{-1}. In contrast to these studies using DSC, we are able, in the present work using DRS, to observe the changes that occur in the molecular dynamics of a system during reaction. It was found possible to estimate T_F for the present system from an analysis of the behaviour of the α-relaxation at different values of T_R. Table 2 lists the plateau values ($\log f_{mp}$ say) of $\log f_{max}$ determined from Fig. 17b for $T_R \geq 75$°C and includes values for $\log f_{mp}$ at 60, 65 and 70°C estimated by linear extrapolation of the higher temperature data. Values of $\log f_{max}$(obs) at different values of $\log t_r$ for T_R equal to 60, 65 and 70°C are shown in Table 3. Plots were made of: (i) $\log f_{mp}$ vs. T_R; and (ii) $\log f_{max}$(obs) vs. T_R at fixed values of $\log t_r$. For $T_R > 72 \pm 1$°C $\log f_{max}$(obs) falls with time to a plateau value as the elastomer is formed. For $T_R < 72 \pm 1$°C the $\log f_{max}$(obs) values decrease without limit in our range as the glass is formed. Hence $T_F = 72 \pm 1$°C and $\log f_{mp} = 0.35 \pm 0.15$ at $T_R = T_F$ for this system. Thus the DRS measurements have provided a direct method for determining T_F for this boroxine/epoxide mixture. In Section 6 we discuss how T_F is related to the behaviour of the glass transition temperature T_g during reaction.

Tombari and Johari [9] used DRS at 1 kHz to study the

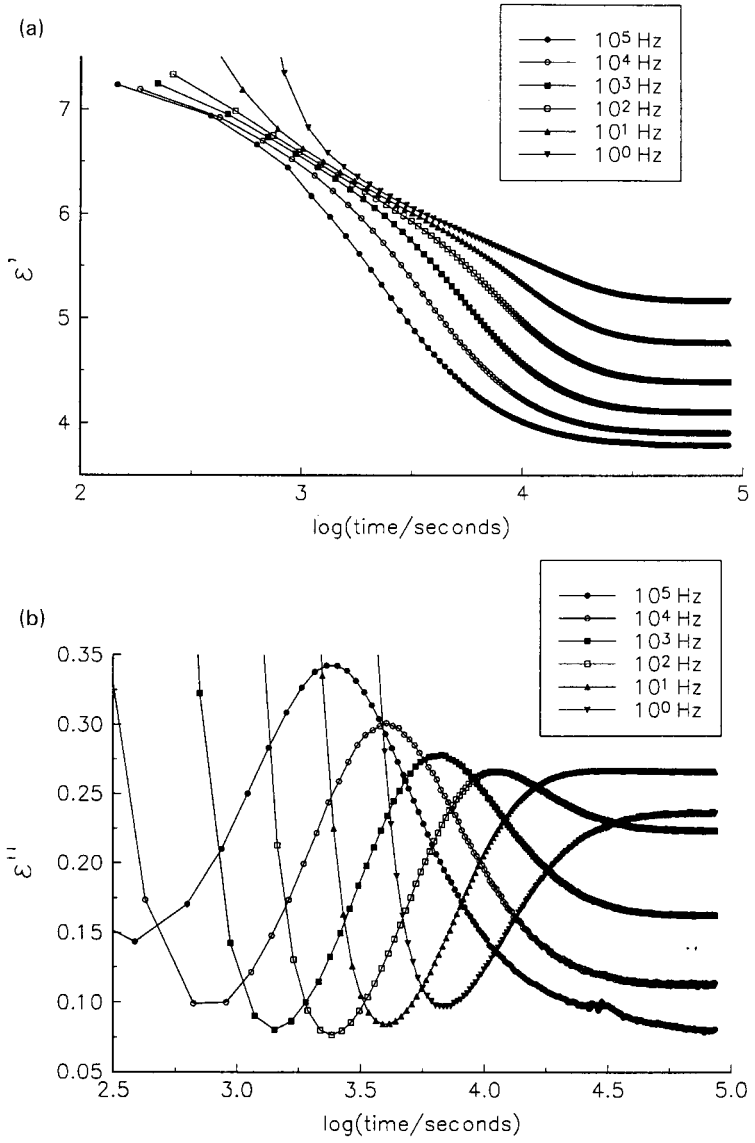

Fig. 14. (a) ε' and (b) ε'' vs. log(t/s) at fixed measuring frequencies for $T_R = 80°C$.

curing of hexylamine with a diepoxide (DGEBA) at 306.2 and 316.2 K. Their loss data at 306.2 K are similar to those shown here in Fig. 12 for $T_R = 60°C$ while their data at 316.2 K are similar to those shown in Fig. 14 at low frequencies for $T_R = 80°C$. i.e. the loss values tend to plateau at long times. Their single-frequency-data for the reaction at 316.2 K indicate elastomer-formation but are insufficient to demonstrate the constancy of ε'' vs. $\log f$ plots at long times.

6. Spectral line-shape of the α-process

Fig. 18 shows normalised plots of $\varepsilon''/\varepsilon''_{max}$ vs. $\log(f/f_{max})$ for the products obtained for $75 \leq T_R \leq 100°C$. The loss curves are very broad (e.g. in Fig. 13b, for $\log t_r = 10$ ks the width at half height $\Delta_{1/2} \approx 4.45$) and are asymmetrical in the KWW [19] or Davidson-Cole [20] sense but we have not used these functions to fit our data. The loss curves have $\Delta_{1/2}$ in the range 4.7–5.0, values that are greater than those for the α-relaxation in amorphous polymers, where $\Delta_{1/2}$ values normally lie in the range 1.7–2.5 [20]. It is well established, both experimentally and theoretically, that topological inhomogeneities exist in polymer networks formed from multifunctional reactants [29–33]. Thus, dipole relaxation of equivalent chemical groups may differ in rate since the groups may occur in different local environments. Dipole groups of different chemical structure will also have different relaxation rates. These factors enhance the breadth of the loss peak over that observed for amorphous solid polymers. Glatz-Reichenbach et al. [34] showed that $\Delta_{1/2}$ for the dielectric α-processes in styrene–butyl acrylate (St–BA) copolymers increased

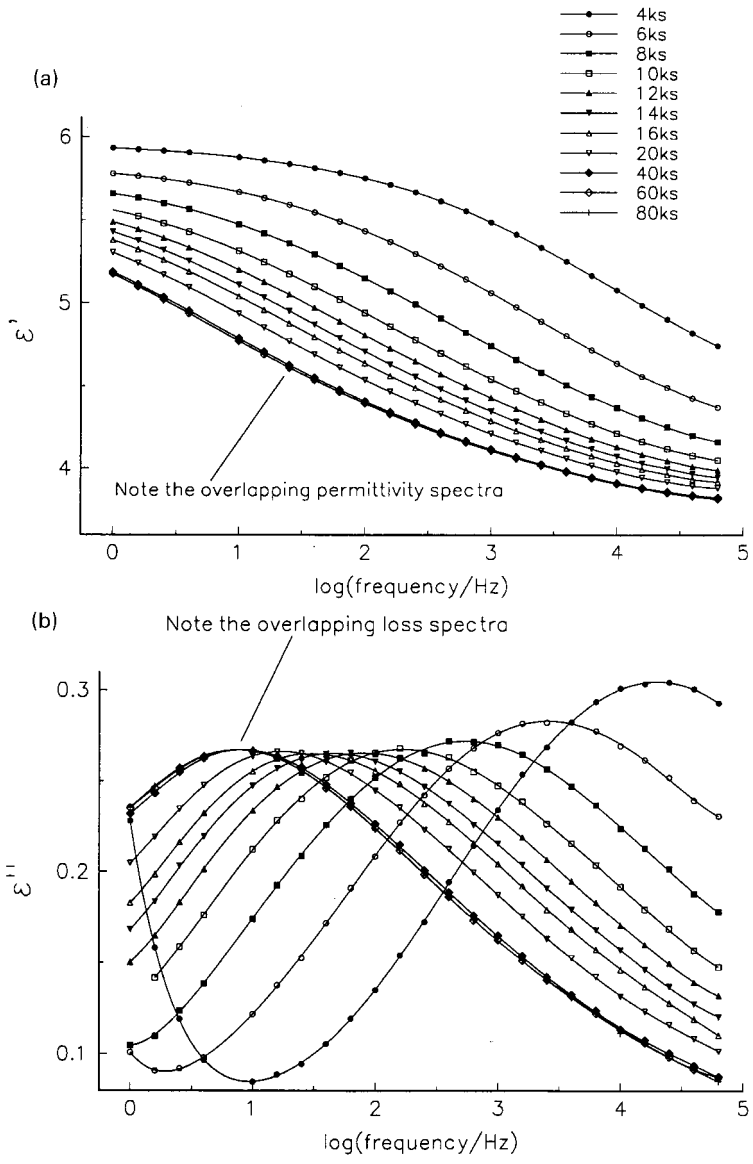

Fig. 15. (a) ε' and (b) ε'' vs. log(f/Hz) at fixed times for $T_R = 80°C$.

from ~3 to 4.5 on going from 0 to 10% (w/w) cross-linking agent. The loss curves for the non-cross-linked material were of KWW form but became more symmetrical on going to cross-linked material [34]. This suggests that motions of dipoles in the vicinity of cross-links in St–BA copolymers are slower than those in the remainder of the system, so make their contribution on the low frequency side of the loss peak, lessening the asymmetry of the overall loss curve. The same reasoning applies to the elastomer-products studied here, so we conclude that the large breadth of the α-relaxation curves (Fig. 18) arises from a superposition of loss curves of different relaxation strengths and relaxation functions from dipole groups that are found in a variety of local environments. Eqs. (A5a) and (A5c) show how these groups make their contribution to the relaxation strength A_α and relaxation function S_α.

7. Alternative representations of the data

Mijovic and coworkers (e.g. Refs. [31–35]) have used the complex impedance $Z(= Z' + iZ'')$ representation of real-time DRS data for thermosetting systems during reaction. We converted our ε-data into this form and Fig. 19 shows, as one example of the results, plots of $\log(-Z''(f))$ vs. $\log(f/\text{Hz})$ for different values of t_r for reaction at 60°C. Similar plots were obtained at other values of T_R. They are similar to those reported for epoxide systems by Mijovic, who has explained that such plots exhibit three zones generally. At the lowest frequencies (Zone A) electrode-polarisation effects dominate and $|Z''|$ increases markedly with decreasing frequency. At higher frequencies (Zone B) ionic conduction dominates, for which a parallel $[R_p,C_p]$ circuit has been proposed [35–39], where the elements R_p, C_p are

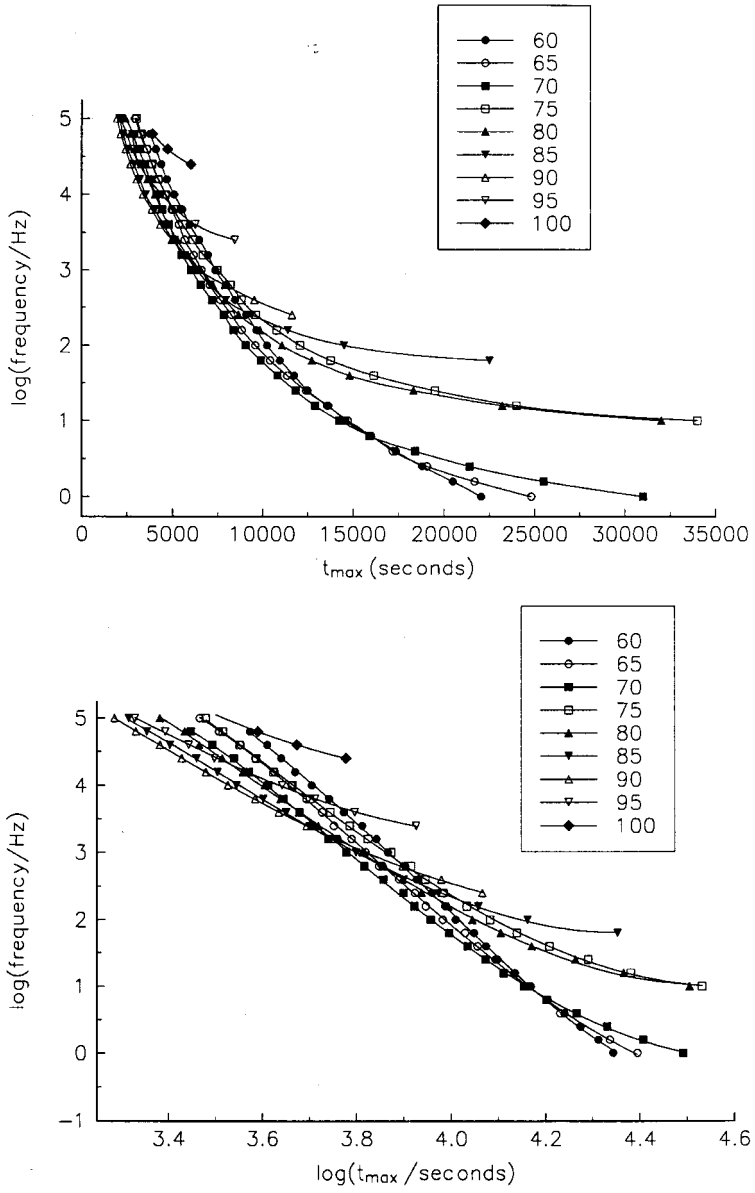

Fig. 16. (a) log(*f*/Hz) vs. t_m/s) as derived from the α-loss curves for reactions in the range $60 \leq T_R \leq 100$°C.

frequency-independent so

$$Z' = \frac{R_p}{1 + \omega^2 R_p^2 C_p^2}; \qquad Z'' = \frac{-\omega R_p^2 C_p}{1 + \omega^2 R_p^2 C_p^2} \tag{4}$$

A peak in Fig. 19 occurs at $\omega_{max} = (R_p C_p)^{-1}$. Also $|Z''_{max}| = R_p/2$ so R_p and C_p can be determined from ω_{max} and Z''_{max}. At higher frequencies (Zone C) dipole relaxation makes its contribution as a small high-frequency shoulder on the Z'' peak for ion motions. Thus, this representation emphasises the *ionic conduction* processes (zones A and B) in contrast to the ε'' representation that emphasises the *dipole relaxation*process. Note that DRS data during polymerisation may also be presented as the complex modulus ($M = \varepsilon^{-1}$), which in the dipole relaxation region suppresses the conductivity contribution. It may be possible to resolve the relative contributions of electrode polarisation (Zone A) and conduction (Zone B) to M at low frequencies by analysis of the plots of M' and M'' vs. log *f*, but we have not pursued this in this paper. There is little merit in presenting dipole relaxation (Zone C) in terms of *M* since it is ε that is linearly related to a Fourier transform of the molecular dipole correlation function (see Appendix A). The curves in Fig. 19 are dominated by the ionic conduction process (Zone B). As t_r increases the local viscosity increases, decreasing the ionic mobility and hence increasing R_p with time. Values of log $f_{max\ (Z'')}$ were determined for each T_R value. Fig. 20 shows plots of $\log f_{max}(Z'')$ vs. t_r. The conductivity σ and resistivity $\rho(= \sigma^{-1})$ are determined from $\sigma = d/AR_p$ where *A* is the electrode area and d the sample thickness. Fig. 21 shows plots of

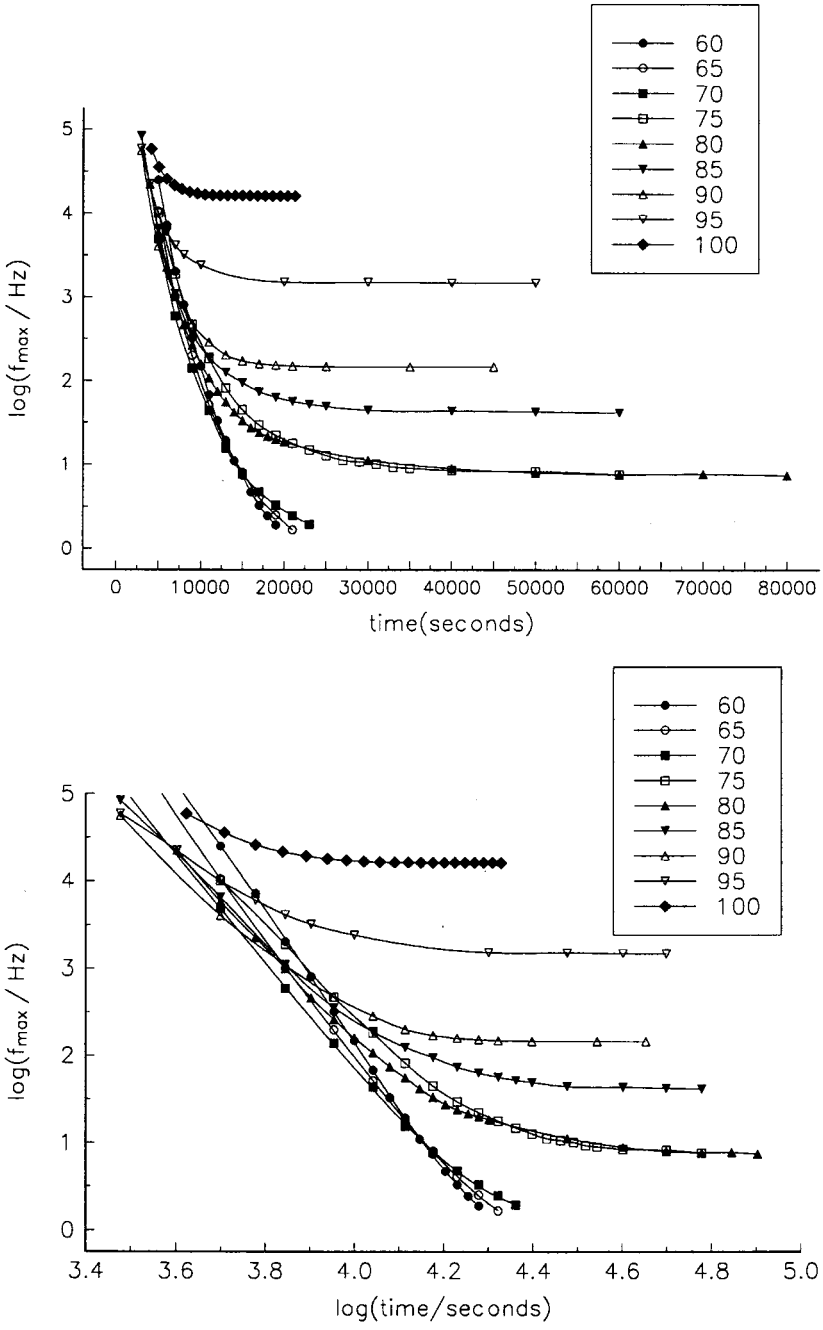

Fig. 17. (a) $\log(f_m/\mathrm{Hz})$ vs. t_r/s and (b) $\log(f_m/\mathrm{Hz})$ vs. $\log(t_r/\mathrm{s})$ for the α-loss curves for reactions in the range $60 \leq T_R \leq 100$°C.

Table 1
Values of $\log f_{max}$ at different times for the reaction at 60°C

t_r/ks	$\log(f_{max}/\mathrm{Hz})$	t_r/ks	$\log(f_{max}/\mathrm{Hz})$	Δ
6	3.75	18	0.30	–
8	2.97	20	0.02	–
10	2.12	30	−0.93	0.39
12	1.50	40	−1.45	0.77
14	1.10	50	−1.74	1.02
16	0.75			

Table 2
Values of $\log(f_{mp})$ at different reaction temperatures

T_R/°C	$\log(f_{mp}/\mathrm{Hz})$	T_R/°C	$\log(f_{mp}/\mathrm{Hz})$(estimated)
100	4.2	70	0 ± 0.15
95	3.15	65	−0.30 ± 0.15
90	2.30	60	−0.60 ± 0.20
85	1.70		
80	0.95		
75	0.85		

Table 3
Estimated values of $\log(f_{max})$ at different values of t_r

T_R/°C	$\log(f_{max}$/Hz) at $\log(t_r$ /s) =			
	4.4	4.6	4.8	5.0
60	−0.05	−1.3	−2.0	−2.4
65	0	−0.5	−1.0	−1.5
70	0.25	0	−0.02	−0.04

$\log(\sigma$/S cm^{-1}) vs. t_r and while the data suggest that limiting behaviour would be obtained at long times as for the ε''-data, the $f_{max}(Z'')$ values at the longest times lie below our range. Comparison of the results for dipole motions (Fig. 17) and ion motions (Fig. 20) shows that at each value of T_R, the values of $f_{max}(Z'')$ (ion motions) fall to 1 Hz in a time shorter than that for $f_{max}(\varepsilon'')$ (dipole motions) to reach that frequency. Thus, molecular mobility is still rapid at times greater than those for which the peak in $\log(-Z'')$ has fallen to 1 Hz.

For reactions conducted at 110 and 120°C (Figs. 10 and 11) only the low frequency side of the loss peak was observable in our range, so the variation in $f_{max}(\varepsilon'')$ with time could not be determined directly. Measurements were made at 100, 110 and 120°C in which the range was extended to ultra-low frequencies in order to examine the behaviour of Z'' at long times. Fig. 22 shows plots of $\log(-Z'')$ vs. $\log(f$/Hz) for fixed reaction times t_r during reaction at 110°C. Similar results were obtained at 100 and 120°C. As before (e.g. Fig. 20) the peaks move to lower frequencies as t_r is increased and at long times the peaks become become independent of t_r. This behaviour is similar to that for f_{max} (ε'') above T_F, as we discussed. Fig. 23 shows plots of $\log(f_{max}$ (Z'')/Hz) vs. t_r for these temperatures. f_{max} decreases from its initial value to become constant at long times. Ionic conduction in the present systems arises from ionic impurities and the dissociated species derived from monomers, polymers and benzyl alcohol. Due to impurities, α-values vary between mixtures of the same initial composition, in contrast to the dipole relaxation properties. We have used the method of Mijovic [35–39] to analyse the kinetic behaviour of ρ in Fig. 23 in terms of the degree of conversion $\alpha(t_r)$ so that

$$\frac{\alpha(t_r)}{\alpha_m} = \frac{\log \rho(t_r) - \log \rho(0)}{\log \rho(\infty) - \log \rho(0)} \quad (5)$$

α_m is the degree of conversion achieved at long times and 0 and ∞ refer to α-values at time zero and at the plateau level, respectively. Fig. 24 shows plots of α/α_m vs. t_r derived from Fig. 23. As T_R is increased the apparent rate of conversion increases. Mijovic and coworkers have shown for several epoxide–amine systems that conversion data derived in this way are in good agreement with those obtained from real-time chemical analysis. Fig. 25 compares the plots of $\log \rho$ vs. t_r and $\log$ (τ_α(vs. t_r at $T_R = 100$°C where $\langle\tau_\alpha\rangle = [2\pi f_{max}(\varepsilon'')]^{-1}$. The conductivity data settle to a constant value at times shorter than those for dipole relaxation. Ionic conduction provides an indirect method for monitoring changes in the molecular composition of the reaction mixture with time. Changes in α with time reflect changes in the mobility of the ions caused by changes in their local environment whereas the ε-data reflect changes in the molecular dynamics of the chain dipoles in the system. It appears in this case that σ is insensitive to changes in the composition as the reaction proceeds at long times. We emphasise that the Z and ε data shown here are simply different representations of the same measured dielectric/electrical properties of the reaction mixture at given values of t_r and T_R, but they place emphasise differently the ion and dipole motions.

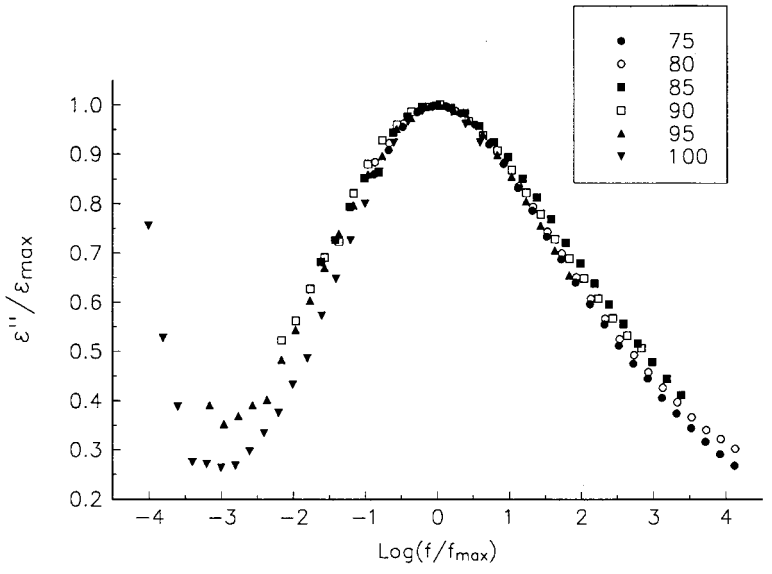

Fig. 18. Normalised loss ($\varepsilon'/\varepsilon''_{max}$) vs. $\log(f/f_{max})$ for the α-process for the products of reactions conducted in the range $75 \le T_R \le 100$°C.

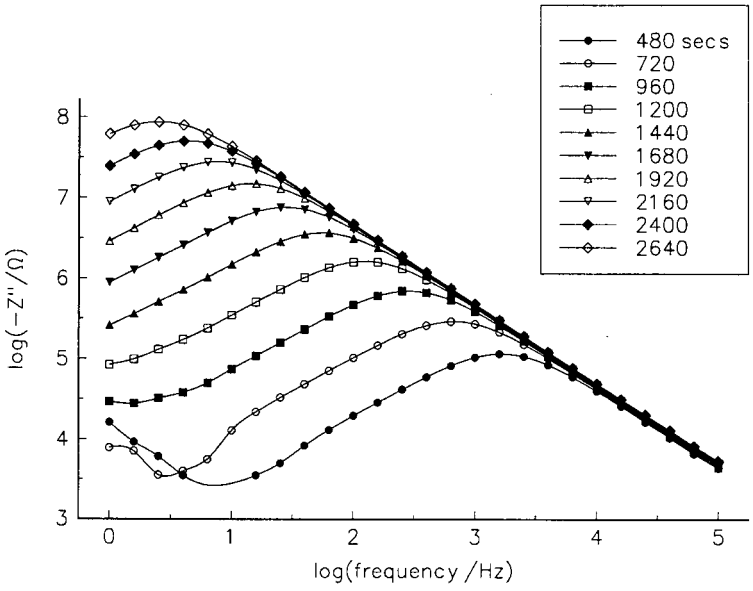

Fig. 19. $\log(-Z''/\Omega)$ vs. $\log(f/\mathrm{Hz})$ at fixed times for reaction at 60°C.

8. Relation to the time–temperature-transition (TTT) diagram

In well-known work Gillham [1,2] constructed a 'TTT' diagram to describe key processes occurring during a thermosetting reaction including gelation, vitrification, full-cure, and, in special cases, phase-separation of products during reaction. We now consider in relation to the present work: (i) the possible detection of the onset of gelation during reaction using DRS measurements; and (ii) the relationship between the DRS behaviour described here to the TTT diagram of Gillham [1,2]. One definition of the onset of chemical gelation of a thermosetting system is that it occurs at the time when the weight-average molecular weight of the system diverges to infinity [40]. On gelation, the system transforms from a viscoelastic liquid, having a zero low frequency shear modulus, to a viscoelastic solid having a non-zero low-frequency shear modulus. For a thermosetting system the transition would occur at the 'gel-time' t_{gel} at a critical extent of cross-linking P_G say. Equilibrium theories by Flory [40] and others [41–43] have been developed to predict P_G for model systems. For example for a epoxide–amine reaction [43]

$$P_G = [1 + rx(f - 2)]^{-1/2} \tag{6}$$

where r is the ratio of the number of epoxide groups to that of the amine hydrogens, f is the functionality of the amine

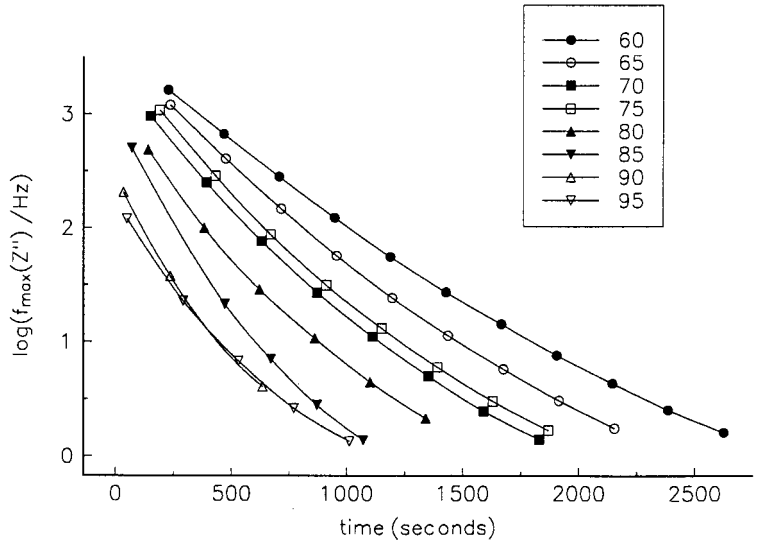

Fig. 20. $\log(f_m(Z'')/\mathrm{Hz})$ vs. t_r/s for $60 \leq T_R \leq 95$°C obtained from impedance plots (e.g. Fig. 19).

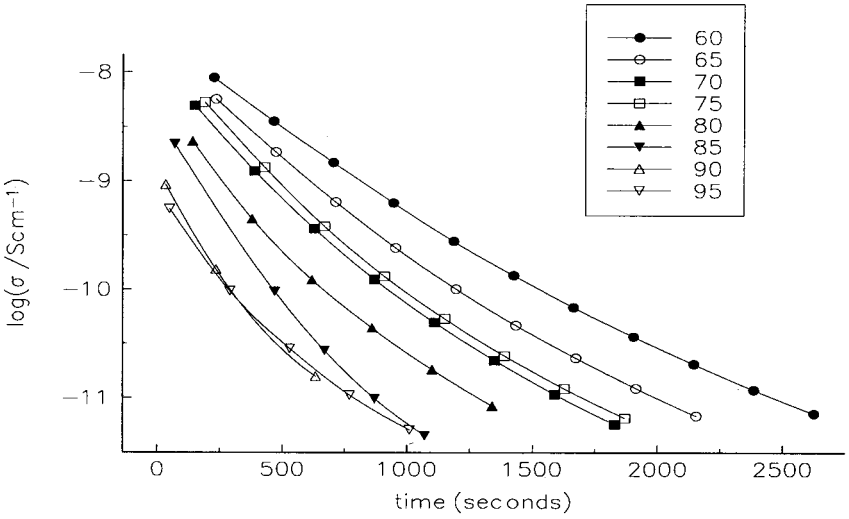

Fig. 21. $\log(\sigma/\mathrm{S\ cm^{-1}})$ vs. t_r/s showing the decrease in α with increasing time for reactions in the range $60 \leq T_R \leq 95$°C.

and x is the fraction of amine hydrogens in the mixture. For a stoichiometric mixture of a diepoxide a diamine $f = 4$, $r = 1, x = 1$ so $P_G = 0.577$. In the application of this theory the measured extent of reaction is assumed to be equal to the extent of cross-linking, but this is not the case generally. Furthermore, direct measurement of the extent of cross-linking is difficult to achieve. In alternative approaches involving dynamical quantities [44], the time t_{gel} is often quoted as being the time at which a particular feature is observed in the dynamic-mechanical properties of the evolving system. These are e.g. (i) the time at which the steady shear viscosity diverges; (ii) the time at which the real part (G') and the imaginary part (G'') of the dynamic shear modulus become equal (known as the $G' - G''$ crossover point) at a fixed measing frequency; and (iii) the time at which a peak occurs in $\tan\delta$ (mechanical) $= G''/G'$ for a fixed measuring frequency. These have been discussed critically by Winter [44]. For (ii) it was shown that the crossover occurs for materials that exhibiting a power-law-dependence $G(t_r) \sim t_r^{-n}$ with $n = 1/2$. Mijovic and coworkers [39] have compared (i), (ii) and (iii) for an epoxide–amine system and added a further method (iv) where t_{gel} is given as the time at which the first step in a plot of Z'' vs. t_r occurs at the fixed measuring frequency. Good agreement was reported between t_{gel}-values obtained by methods (i) to (iv). However, caution is needed since, in addition to the reasons given by Winter [44], these values of t_{gel} will depend on the frequency of measurement. Thus, gel-times derived from (i) to (iv) serve as *operational gel-times* with respect to the frequency of measurement. Ionic conductivity has also been proposed as a means of measuring t_{gel}. This has the advantage that the d.c. conductivity is independent of frequency. Johari and coworkers [45,46] used empirical equations to extrapolate plots of $\log \alpha(t_r)$ vs. t_r to give

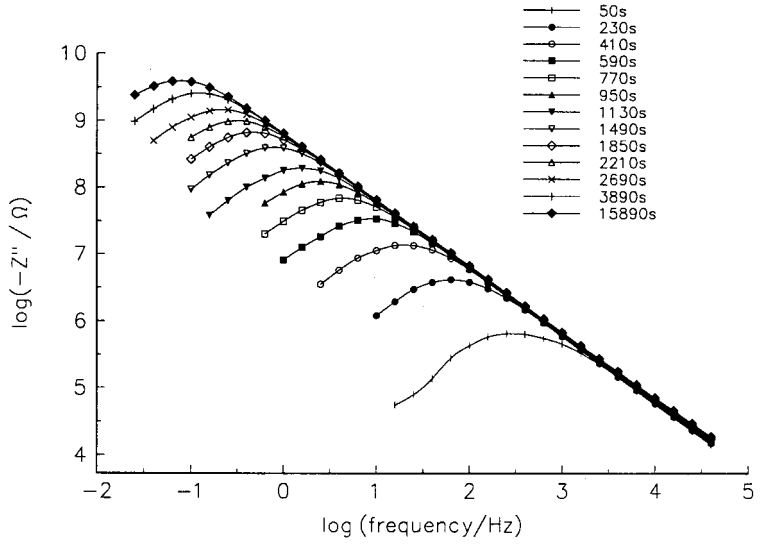

Fig. 22. $\log(-Z'')$ vs. $\log(f/\mathrm{Hz})$ at fixed times during reaction at 110°C.

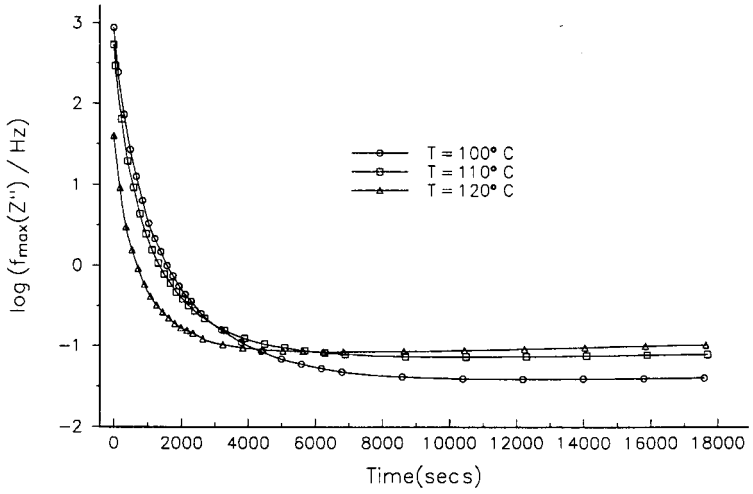

Fig. 23. $\log(f_m(Z'')/\text{Hz})$ vs. t_r/s obtained from impedance data (e.g. Fig. 22) for $100 \leq T_R \leq 120$°C.

times at which $\alpha(t_r)$ would become effectively zero to define the gel-time for the reaction. As pointed out by Zukas [47] and by Mijovic and coworkers [38], extrapolation of ionic conductivity data is not appropriate and there is no reason why the diffusion of ions would stop at the onset of gelation. A further method (v) suggested by Mijovic and coworkers [38] takes the point of inflection in plots of log σ vs. t_r to indicate a gel-time. The inflection-point gives the maximum rate of change of ionic conductivity during cure. For a TGEPA/MDA thermoset they found good agreement between the apparent gel-times derived from (i) to (v). However, the gel-times derived from (i) to (iv) will vary with measurement frequency so the agreement will not hold generally. Our DRS measurements give no direct evidence for gel-formation. We take the view, in agreement with Zukas [47], that the onset of gelation in a thermosetting system has no corresponding event in the DRS behaviour. The ions sense the local viscosity during their translational motions so the ionic mobility, and hence conductivity, will decrease as the local viscosity increases during reaction irrespective of whether a viscous non-crosslinked polymer or a dense polymer network is formed en-route to the formation of a glass (for $T_R < T_F$) or an elastomer (for $T_R > T_F$). Our conductance data (see Fig. 20) shows no indication of the onset of a gel-point so it seems unlikely that they give any information on the liquid-to-gel transformation in this system.

Following gelation further reaction extends the cross-link density of the network and *either* vitrification will occur if the reaction becomes diffusion-controlled through lack of molecular mobility *or* an elastomer-product will form if chemical reaction is completed. Our DRS results indicate a floor temperature T_F so it is useful to relate our work to that of Gillham [1,2] and to Montserrat [3]. DRS has been used widely to monitor changes in molecular mobility as thermosetting systems approach vitrification (for a recent review see Ref. [8]). In earlier work [11] we modelled the changes in DRS behaviour as the reaction became diffusion-controlled

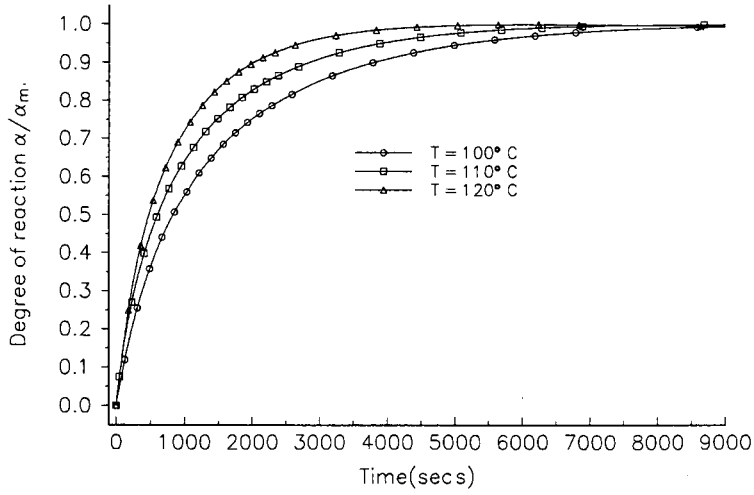

Fig. 24. α/α_m vs. t_r as calculated from the data of Fig. 24 using Eq. (5) of the text.

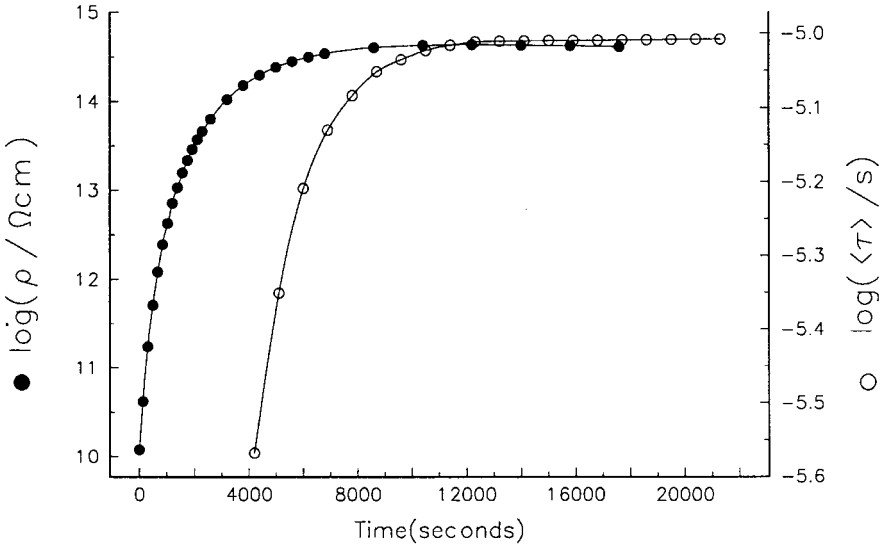

Fig. 25. A comparison of the t-dependent behaviour of log ($\langle\tau_\alpha\rangle$/s) and log($\rho$/Ω cm) for $T_R = 100$°C.

through lack of molecular mobility. In all such studies the 'vitrification time' needs to be defined operationally. As discussed by Angell and coworkers for glass-forming materials [26,48] it is customary to extrapolate the plot of log f_{max} vs. $(T/K)^{-1}$ to $\log f_{max} = -2$ to define the T_g-value operationally. The glass thus prepared is thermodynamically unstable and will relax its thermodynamic properties through physical ageing, which will increase T_g with time. We extend the TTT diagram as follows, to include the variation of T_g with time during reaction at different T_R values. In Fig. 26 we show a schematic plot of T'_g vs. log t_r for different T'_R for a thermosetting system. The time-scale is arbitrary. T'_g is the difference between T_g(reacting mixture) and T_g(unreacted mixture). Here T_g is measured by a dynamical technique (e.g. DRS, DSC or DMTA)) and refers to a fixed effective measuring frequency. The 'normalised temperature T'_R is the difference between T_R and T_g(unreacted mixture). We set $T'_F = 70$ in the figure so for reactions conducted above T'_F an elastomer is formed, the reaction goes to chemical completion and all products have the same T_g. For $T'_R < 0$ the reaction mixture is a glass so little reaction occurs, whose rate diminish further as T'_R is decreased. For $T'_R > 0$, T'_g increases during reaction to a near-plateau level at which T_g(plateau) $= T_g$, i.e. a polymer glass is formed whose T_g − value $\approx T'_R$, but some further reaction will occur slowly at longer times, increasing T_g slightly.

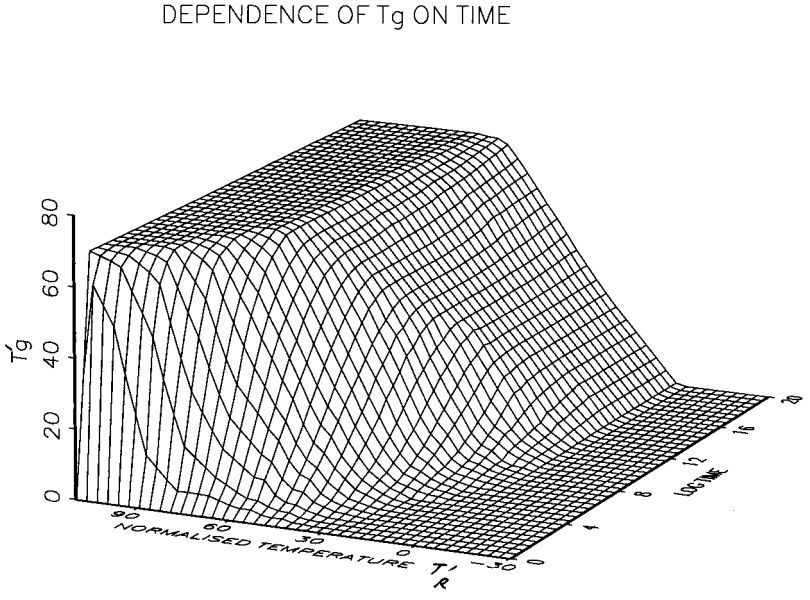

Fig. 26. Schematic plot of the variation of the glass transition temperature with time during isothermal curing indicating (a) the rise in T_g during reaction and the occurrence of a 'floor temperature'. T'_g and 'normalised temperature' are defined in the text.

This pattern of behaviour continues until $T'_R = T'_F = 70$, above which the T_g -value equals 70 for all products. For $T'_R \geq 70$, increase in T'_R simply increases the rate at which the T_g-curve rises to the plateau level. The figure shows how the T_g of a thermosetting reaction mixture varies with time and demonstrates the connections between T_g and T_F. Thus Fig. 26 extends the TTT diagram of Gillham to include the *floor temperature* T_F as we have deduced from our analyses of the DSC studies of Montserrat [3] and the present DRS studies for thermosetting systems.

Acknowledgements

The authors thank EPSRC for a Case Award to I.K.S. and for a grant for the purchase of the Novocontrol Dielectric Spectrometer. G.W. thanks The Leverhulme Trust for an Emeritus Fellowship.

Appendix A

If, at time t_r during reaction, the time correlation functions for dipole motions decay to zero in a time-scale shorter than that required to change the chemical composition of the reaction mixture by a significant amount then the dipole moment correlation function $[\Phi_\mu(t)]_{t_r}$ for all dipoles in a macroscopic volume V of the reaction mixture at time t_r is given by

$$[\Phi_\mu(t)]_{t_r} = \Big[\sum_i \sum_i [\langle \vec{\mu}_i(0)\cdot\vec{\mu}_j(t)\rangle\Big]_{t_r} / \sum_i \sum_j [\langle \vec{\mu}_i(0)\cdot\vec{\mu}_j(0)\rangle]_{t_r} \tag{A1}$$

where $\vec{\mu}_i(t)$ is the dipole moment of species i at time t given its value was $\vec{\mu}_i(0)$ at $t = 0$, and the sums are taken over all dipole species. $\langle\cdots\rangle$ indicates a statistical average. For the case where there are no angular correlations between dipoles this becomes

$$[\Phi_\mu(t)]_{t_r} = \sum_i c_i(t_r)\mu_i^2 [\Phi_{\mu_i}(t)]_{t_r} / \sum_i c_i(t_r)\mu_i^2 \tag{A2}$$

where $c_i(t_r)$ is the concentration of species i at t_r, and $[\Phi_i(t)]_{t_r} = [\langle \vec{\mu}_i(0).\vec{\mu}_i(t)\rangle/\mu_i^2]_{t_r}$ is the normalised autocorrelation function for the reorientational motions of species i at time t_r. Thus the dielectric relaxation behaviour gives a snapshot of the dynamics of the system at t_r. The occurence of α and β processes in the f-domain can be rationalised within one general scheme for partial (β) and total (α) relaxations of the dipole vectors associated with all of the species. Following Williams [15,16] we write the dipole moment correlation function for the motions of species i as

$$[\Phi_{\mu_i}(t)]_{t_r} = \Big\{\varphi_{\alpha_i}(t)\Big[\sum_{r_i} p_{r_i} q_{r_i} + \sum_{r_i} p_{r_i}(1 - q_{r_i})\varphi_{\beta_{r_i}}(t)\Big]_{t_r}\Big\} \tag{A3}$$

where p_{ri} is the probability of obtaining species i in the temporary local environment r_i at $t = 0$. $q_{r_i} = [\langle \vec{\mu}_{ri}\rangle^2]/\mu_i^2$ where $\langle \vec{\mu}_{r_i}\rangle$ is the mean dipole moment for species i residing in environment r_i when the β_{r_i} process is completed in time. $\varphi_{\alpha i}$ and $\varphi_{\beta r_i}(t)$ are the relaxation functions for the α process and the β_ρ process for the species i, as we have described. The sum is taken over all environments r_i for the species i. Combining Eq. (1) of the script with Eqs. (A2) and (A3) we may write for the mixture of species at time t_r

$$\frac{\varepsilon(\omega, t_r) - \varepsilon_\infty(t_r)}{\varepsilon_0(t_r) - \varepsilon_\infty(t_r)} = A_\alpha(t_r)S_\alpha(\omega, t_r) + A_\beta(t_r)S_\beta(\omega, t_r) \tag{A4}$$

where A_j and S_j are the relaxation strength and normalised relaxation function, respectively, for the ith-process (i = α or β) and are given by

$$A_\alpha(t_r) = \Big[\sum_i c_i(t_r)\mu_i^2 \sum_{r_i} p_{r_i} q_{r_i}\Big] / \sum_i c_i(t_r)\mu_i^2 \tag{A5a}$$

$$A_\beta(t_r) = \Big[\sum_i c_i(t_r)\mu_i^2 \sum_{r_i} p_{r_i}(1 - q_{r_i})\Big] / \sum_i c_i(t_r)\mu_i^2 \tag{A5b}$$

$$S_\alpha(\omega, t_r) = 1 - i\omega\Im\Big[c_i(t_r)\mu_i^2 \varphi_{\alpha_i}(t) \sum_{r_i} p_{r_i}(1 - q_{r_i})\Big] / \sum_i c_i(t_r)\mu_i^2 \tag{A5c}$$

$$S_\beta(\omega, t_r) = 1 - i\omega\Im\Big[\sum_i c_i(t_r)\mu_i^2 \sum_{r_i} p_{r_i}(1 - q_{r_i})\varphi_{\beta_{r_i}}(t)\Big] / \sum_i c_i(t_r)\mu_i^2 \tag{A5d}$$

Also the total relaxation strength is given by

$$\Delta\varepsilon(t_r) = \varepsilon_0(t_r) - \varepsilon_\infty(t_r) = F(\varepsilon_0, \varepsilon_\infty) \sum_i c_i(t_r)\mu_i^2 \tag{A5e}$$

where $F(\varepsilon_0, \varepsilon_\infty)$ is a simple function of the limiting permittivities [20].

References

[1] Gillham JK. Polym Engng Sci 1986;26:1430.
[2] Gillham JK, Chan LC, Kinloch AJ, Shaw SJ. Abstr Plastics and Rubber Institute, International Conference on Toughening of Plastics, July 1985.
[3] Montserrat SJ. Appl Polym Sci 1992;44:545.
[4] Kranbuehl DE, Hoff M, Godfrey J, Hoffman R. Polym Engng Sci 1986;26:338.
[5] Senturia SD, Sheppard NF. Adv Polym Sci 1986;80:1.
[6] Mangion MBM, Johari GP. J Polym Sci, Polym Phys Ed 1990;28:71.
[7] Casalini R, Corezzi S, Fioretto D, Livi A, Rolla PA. Chem Phys Lett 1996;258:470.
[8] Williams G, Smith IK, Holmes PA, Varma S. J Phys: Condens Matter 1999;II:A57–74.
[9] Tombari E, Johari GP. J Chem Soc, Faraday Trans 1993;89:3477.
[10] Johari GP. J Chem Soc, Faraday Trans 1994;90:883.
[11] Fournier J, Williams G, Duch C, Aldridge GA. Macromolecules 1996;29:7097.
[12] Cassettari M, Salvetti G, Tombari E, Veronesi S, Johari GP. J Mol Liq 1993;56:141.

[13] Cassettari M, Salvetti G, Tombari E, Veronesi S, Johari GP. J Non-Cryst Solids 1994;172–174:554.
[14] Casalini R, Corezzi S, Fioretto D, Livi A, Rolla PA. Chem Phys Lett 1996;258:470.
[15] Williams G. Chem Rev 1972;72:55.
[16] Williams G. Chem Soc Rev 1978;7:89.
[17] Mangion MBM, Johari GP. J Polym Sci, Polym Phys Ed 1990;28:1621.
[18] Mangion MBM, Johari GP. Macromolecules 1990;23:3687.
[19] Williams G, Watts DC. Trans Faraday Soc 1970;30:80.
[20] McCrum NG, Read BE, Williams G. Anelastic and dielectric effects in polymeric solids. New York: Dover, 1991.
[21] Butta E, Levi A, Levita G, Rolla PA. J Polym Sci, Polym Phys Ed 1995;33:2253.
[22] Johari GP, McAnaman JG, Wasylyshyn DA. J Chem Phys 1996;105:1054.
[23] Ferry JD. Viscoelastic properties of polymers. 2nd ed. New York: Wiley, 1970.
[24] Matsuoka S. Relaxation phenomena in polymers. Munich: Hanser, 1992.
[25] Matsuoka S, Williams G, Johnson GE, Anderson EW, Furukawa T. Macromolecules 1985;18:2652.
[26] Ediger MD, Angell CA, Nagel SR. J Phys Chem 1996;31:13 200.
[27] Williams G. Trans Faraday Soc 1964;60:1556.
[28] Williams G. Adv Polym Sci 1979;33:60.
[29] Matsuo ES, Orkisz M, Sun S-T, Li Y, Tanaka T. Macromolecules 1994;27:6791.
[30] Dusek K. Angew Makromol Chem 1996;240:1.
[31] Panyukov S, Rabin Y. Macromolecules 1996;29:7960.
[32] Dusek K, Somvarsky J. Macromol Symp 1996;106:119.
[33] Rabin Y, Panyukov S. Macromolecules 1997;30:301.
[34] Glatz-Reichenbach JKW, Sorriero LJ, Fitzgerald JJ. Macromolecules 1994;27:1338.
[35] Mijovic J, Yee CFW. Macromolecules 1994;27:7287.
[36] Bellucci F, Valentino M, Monetta T, Nicodemo L, Kenny J, Nicolais L, Mijovic J. J Polym Sci, Polym Phys 1994;32:2519.
[37] Bellucci F, Valentino M, Monetta T, Nicodemo L, Kenny J, Nicolais L, Mijovic J. J Polym Sci, Polym Phys 1995;33:433.
[38] Mijovic J, Andjelic S, Fitz B, Zurawsky W, Mondragon I, Bellucci F, Nicolais L. J Polym Sci, Polym Phys 1996;34:379.
[39] Mijovic J, Bellucci F, Nicolais L. J Electrochem Soc 1995;142:1176.
[40] Flory PJ. Principles of polymer chemistry. Ithaca, New York: Cornell University Press, 1953.
[41] Gordon M, Malcolm GN. Proc R Soc Lond A 1966;295:29.
[42] Miller DR, Macosko GW. Macromolecules 1978;11:656.
[43] Huang ML, Williams JG. Macromolecules 1994;27:7423.
[44] Winter HH. Polym Engng Sci 1986;27:1698.
[45] Mangion MBM, Johari GP. J Polym Sci, Polym Phys Ed 1991;29:1117.
[46] Parthun MG, Johari GP. J Polym Sci, Polym Phys Ed 1992;30:655.
[47] Zukas WX. Macromolecules 1993;26:2390.
[48] Green JL, Ito K, Xu K, Angell CA. J Phys Chem B 1999;10:3991.